

1 **Soil related developments of the Biome-BGCMuSo v6.2**
2 ~~terrestrial ecosystem model by integrating crop model~~
3 ~~components~~

5 Dóra Hidy^{1,2*}, Zoltán Barcza^{1,3,4}, Roland Hollós^{3,5}, Laura Dobor^{1,4}, Tamás Ács⁶, Dóra
6 Zacháry⁷, Tibor Filep⁷, László Pásztor⁸, Dóra Incze³, Márton Dencső^{8,9}, Eszter Tóth⁸,
7 Katarína Merganičová^{4,109}, Peter Thornton¹¹Thornton⁴⁰, Steven Running¹²Running⁴⁴, Nándor
8 Fodor^{4,5}

9

10 ¹ Excellence Center, Faculty of Science, ELTE Eötvös Loránd University, H-2462 Martonvásár, Hungary
11 ² MTA-MATE Agroecology ResearchReeearch Group, Department of Plant Physiology and Plant Ecology,
12 Hungarian University for Agriculture and Life SciencesMTA-MATE, H-2100 Gödöllő, Hungary

13 ³ Department of Meteorology, Institute of Geography and Earth Sciences, ELTE Eötvös Loránd University,
14 H-1117 Budapest, Hungary

15 ⁴ Faculty of Forestry and Wood Sciences, Czech University of Life Sciences Prague, 165 21 Prague, Czech
16 Republic["]

17 ⁵ Centre for Agricultural Research, Agricultural Institute, H-2462 Martonvásár, Hungary

18 ⁶ Department of Sanitary and Environmental Engineering, Budapest University of Technology and Economics,
19 H-1111 Budapest, Hungary

20 ⁷ Geographical Institute, ResearchReeearch Centre for Astronomy and Earth Sciences, H-1112 Budapest,
21 Hungary

22 ⁸ Institute for Soil Sciences, Centre for Agricultural Research, H-1022 Budapest, Hungary

23 ⁹ Doctoral School of Environmental Sciences, ELTE Eötvös Loránd University, H-1117 Budapest, Hungary

24 ¹⁰⁹ Department of Biodiversity of Ecosystems and Landscape, Institute of Landscape Ecology, Slovak Academy
25 of Sciences, SK 949 01 Nitra, Slovakia

26 ¹¹⁴⁰ Climate Change Science Institute/Environmental Sciences Division, Oak Ridge National Laboratory, Oak
27 Ridge, TN 37831, USA

28 ¹²⁴⁴ Numerical Terradynamic Simulation Group, Department of Ecosystem and Conservation Sciences
29 University of Montana, Missoula, MT 59812, USA

30

31 *Correspondence to:* Dora Hidy (dori.hidy@gmail.com)

32 **Abstract**

33 Terrestrial biogeochemical models are essential tools to quantify climate-carbon cycle
34 feedback and plant-soil relations from local to global scale. In this study, theoretical basis is
35 provided for the latest version of Biome-BGCMuSo biogeochemical model (version 6.2).
36 Biome-BGCMuSo is a branch of the original Biome-BGC model with a large number of
37 developments and structural changes. Earlier model versions performed poorly in terms of
38 soil water content (SWC) dynamics in different environments. Moreover, lack of detailed
39 nitrogen cycle representation was a major limitation of the model. Since problems associated
40 with these internal drivers might influence the final results and parameter estimation,
41 additional structural improvements were necessary. ~~During the developments we took
42 advantage of experiences from the crop modeller community where internal process
43 representation has a long history.~~ In this paper the improved soil hydrology and soil
44 carbon/nitrogen cycle calculation methods are described in detail. Capabilities of the
45 Biome-BGCMuSo v6.2 model are demonstrated via case studies focusing on soil hydrology,
46 soil nitrogen and soil organic carbon cyclecontent estimation. Soil hydrology related results
47 are compared to observation data from an experimental lysimeter station. The results indicate
48 improved performance for Biome-BGCMuSo v6.2 compared to v4.0 (explained variance
49 increased from 0.121 to 0.8 for SWC, and from 0.084 to 0.46 for soil evaporation; bias
50 changed from -0.047 to -0.007 $\text{m}^3 \text{m}^{-3}$ for SWC, and from -0.68 mm day^{-1} to -0.2 mm day^{-1}
51 for soil evaporation). Nitrogen balance and soil CO_2 efflux related simulations were evaluated
52 based on observations made in a long-term field experiment under crop rotation. The results
53 indicated that the model is able to provide realistic nitrate content estimation for the topsoil.
54 Soil nitrous oxide (N_2O) efflux and soil respiration simulations were also realistic with overall
55 correspondence with the observations (for the N_2O efflux simulation bias was between -0.13
56 and -0.1 $\text{mg N m}^{-2} \text{ day}^{-1}$, NRMSE was 32.4% – 37.6%; for CO_2 efflux simulations bias was
57 0.04 – 0.17 $\text{g C m}^{-2} \text{ day}^{-1}$, while RMSE was 34.1% – 40.1%). Sensitivity analysis and
58 optimization of the decomposition scheme is presented to support practical application of the
59 model. The improved version of Biome-BGCMuSo has the ability to provide more realistic
60 soil hydrology representation and nitrification/denitrification process estimation which
61 represents a major milestone.

62

63

64 **1. Introduction**

65 The construction and development of biogeochemical models (BGM) is the response
66 of the scientific community to address challenges related to climate change and human
67 induced global environmental change. BGMs can be used to quantify future climate-
68 vegetation interaction including climate-carbon cycle feedback, and as they simulate plant
69 production, they can be used to study a variety of ecosystem services that are related to human
70 nutrition and resource availability (Asseng et al., 2013; Bassu et al., 2014; Huntzinger et al.,
71 2013). Similarly to the models describing various and complex environmental
72 ~~processes~~processes, the structure of biogeochemical models reflects our current knowledge
73 about a complex system with many internal processes and interactions.

74 Processes of the atmosphere-plant-soil system take place on different temporal (sub-
75 daily to centennial) scales and are driven by markedly different mechanisms that are
76 quantified by a large diversity of modeling tools (Schwalm et al., 2019). Plant photosynthesis
77 is an enzyme-driven biochemical process that has its own mathematical equation set and
78 related parameters (and a large literature; e.g. Farquhar et al., 1980; Medlyn et al. 2002; Smith
79 and Dukes, 2013; Dietze, 2013). Allocation of carbohydrates in the different plant
80 compartments is studied extensively and also has a large literature and mathematical tool set
81 (Friedlingstein et al., 1999; Olin et al., 2015; Merganičová et al., 2019). Plant phenology is
82 quantified by specific algorithms that are rather uncertain components of the models
83 (Richardson et al., 2013; Hufkens et al., 2018; Peaucelle et al., 2019). Soil biogeochemistry is
84 driven by microbial and fungal activity and also has its own methodology and a vast literature
85 (Zimmermann et al 2007; Kuzyakov, 2011; Koven et al., 2013; Berardi et al., 2020).
86 Emerging scientific areas like the quantification of the dynamics of non-structural
87 carbohydrates (NSC) in plants has a separate methodology that claims for mathematical
88 representation in models (Martínez-Vilalta et al., 2016). Simulation of land surface hydrology
89 including evapotranspiration is typically handled by some variant of the Penman-Monteith
90 equation that is widely studied thus represents a separate scientific field (McMahon et al.,
91 2013; Doležal et al., 2018).

92 Putting all together, if we are about to construct and further improve a biogeochemical
93 model to consider novel findings and track global changes, we need a comprehensive
94 knowledge that integrates many, almost disjunct scientific fields. Clearly, transparent and
95 well-documented development of a biogeochemical model is of high priority but challenging

96 from the very beginning that claims for cooperation of researchers from various scientific
97 fields.

98 Continuous model development is inevitable but it has to be supported by extensive
99 comparison with observations and some kind of implementation of the model-data fusion
100 approach (Keenan et al., 2011). It is well documented that structural problems might trigger
101 incorrect parameter estimation that might be associated with distorted internal processes
102 (Sándor et al., 2017; Martre et al., 2015). In other words, one major issue with BGMs (and in
103 fact with all models using many parameters) is the possibility to get good simulation results
104 for wrong reasons (which means incorrect parameterization) due to compensation of errors
105 (Martre et al., 2015). In order to avoid this issue, any model developer team has to make an
106 effort to focus also on internal ecosystem conditions (e.g. soil volumetric water content
107 (SWC), nutrient availability, stresses, etc.) and other processes (e.g. decomposition) rather
108 than the main simulated processes (e.g. photosynthesis, evapotranspiration).

109 Historically, biogeochemical models have been developed to simulate the processes of
110 undisturbed ecosystems with simple representation of the vegetation (Levis, 2010). As the
111 focus was on the carbon cycle, water and nitrogen cycles and related soil processes were not
112 well represented. Incorrect representation of SWC dynamics is still an issue with the models
113 especially in drought-prone ecosystems (Sándor et al., 2017). Additionally, human
114 intervention representation (management) ~~is still incomplete in was missing in many cases and~~
115 ~~it seems that~~ some state-of-the-art BGMs, ~~still lack the representation of~~ e.g. thinning, grass
116 mowing, grazing, ~~tillage fertilization, planting or irrigation is missing in some models (see~~
117 ~~harvest (Table A1 in Friedlingstein et al., 2020) 2010~~.

118 In contrast, crop models with different complexity were used for about 50 years or so
119 to simulate the processes of managed vegetation (Jones et al., 2017; Franke et al., 2020). As
120 the focus of the crop models is on final yield due to economic reasons, the carbon balance, or
121 the full greenhouse gas balance was not, or was just partially addressed originally. Crop
122 models typically have a sophisticated representation of soil water balance with a multilayer
123 soil module that usually calculates plant response to water stress as well. Nutrient stress, soil
124 conditions during planting, consideration of multiple phenological phases, heat stress during
125 anthesis, vernalization, manure application, fertilization, harvest, and many other processes
126 have been implemented during the decades (Ewert et al., 2015). Therefore, it seems to be
127 straightforward to exploit the benefits of crop models and implement sound and well-tested
128 algorithms into the BGMs.

129 | ~~Our group has been developing Biome-BGCMuSo for 15 years.~~ Starting from the
130 | well-known Biome-BGC model originally developed to simulate undisturbed forests and
131 | grasslands, using a simple single layer soil submodel (Running and Hunt, 1993; Thornton and
132 | Rosenbloom, 2005), we developed a complex, more sophisticated model (Hidy et al., 2012;
133 | 2016). Biome-BGCMuSo v4.0 (Biome-BGC with Multilayer Soil module) uses a 7-layer soil
134 | module and is capable of simulating different ecosystems from natural grassland to cropland
135 | including several management options (mowing, grazing, thinning, planting and harvest),
136 | taking into account many environmental effects (Hidy et al., 2016). The developments
137 | included improvements regarding both soil and plant processes. In a nutshell, the most
138 | important, soil related developments were the improvement of the soil water balance module
139 | by implementing routines for estimating percolation, diffusion, pond water formation and
140 | runoff; the introduction of multilayer simulation for belowground processes in a simplified
141 | way. The most important, plant related developments involved the implementation of a
142 | routine for estimating the effect of drought on vegetation growth and senescence; the
143 | improvement of stomatal conductance calculation considering atmospheric CO₂
144 | concentration; the integration of selected management modules; the implementation of new
145 | plant compartments (e.g. yield); the implementation of C4 photosynthesis routine; the
146 | implementation of photosynthesis and respiration acclimation of plants and temperature-
147 | dependent Q10; and empirical estimation of methane and nitrous oxide soil efflux.

148 | Problems found with the Biome-BGCMuSo v4.0 simulation result (~~namely such as~~ the
149 | poor representation of soil water content: ~~(Hidy et al., 2016; Sándor et al., 2017)~~ or the lack of
150 | sophisticated, layer-specific soil nitrogen dynamics representation; ~~or~~ and the model structure
151 | related problems, ~~such as the rubber parameterization of the model~~) marked the path for
152 | further developments.

153 | The aim of the present study is to provide detailed documentation on the current,
154 | improved version of Biome-BGCMuSo v6.2, which has many new features and facilitates
155 | various in-depth investigations of ecosystem functioning. Due to large number of
156 | developments, this paper focuses only on the soil related model improvements. Case studies
157 | are also presented to demonstrate the capabilities of the new model version and to provide
158 | guidance for the model user community.

160 **2. The original Biome-BGC model**

161 Biome-BGC was developed from the Forest-BGC mechanistic model family in order
162 to simulate vegetation types other than forests. Biome-BGC was one of the earliest
163 biogeochemical models that included explicit carbon and nitrogen cycle modules. Biome-
164 BGC simulates the storages and fluxes of water, carbon, and nitrogen within and between the
165 vegetation, litter, and soil components of terrestrial ecosystems. It uses a daily time step, and
166 is driven by daily values of maximum and minimum temperatures, precipitation, solar
167 radiation, and vapor pressure deficit (Running and Hunt, 1993). The model calculations apply
168 to a unit ground area that is considered to be homogeneous.

169 The three most important components of the model are the phenological, the carbon
170 uptake and release, and the soil flux modules. The core logic that is described below in this
171 section remained intact during the developments. The phenological module calculates foliage
172 development that affects the accumulation of C and N in leaf, stem (if present), root and
173 consequently the amount of litter. In the carbon flux module gross primary production (GPP)
174 of the biome is calculated using Farquhar's photosynthesis routine (Farquhar et al., 1980) and
175 the enzyme kinetics model based on Woodrow and Berry (2003). Autotrophic respiration is
176 separated into maintenance and growth respiration. Maintenance respiration is calculated as
177 the function of the N content of living plant pools, while growth respiration is an adjustable
178 but fixed proportion of the daily GPP. The single-layer soil module simulates the
179 decomposition of dead plant material (litter) and soil organic matter, N mineralization and N
180 balance in general (Running and Gower, 1991). The soil module uses the so-called
181 converging cascade method (Thornton and Rosenbloom, 2005) to simulate decomposition,
182 carbon and nitrogen turnover, and related soil CO₂ efflux.

183 The simulation has two basic steps. During the first (optional) spinup simulation the
184 available climate data series is repeated as many times as it is required to reach a dynamic
185 equilibrium in the soil organic matter content to estimate the initial values of the carbon and
186 nitrogen pools. The second, normal simulation uses the results of the spinup simulation as
187 initial conditions and runs for a given, predefined time period (Running and Gower 1991). So-
188 called transient simulation option (which is the extension of the spinup routine) is a novel
189 feature in Biome-BGCMuSo [v6.2 relative to the previous versions](#) in order to ensure smooth
190 transition between the spinup and normal phase (Hidy et al., 2021).

191 In Biome-BGC, the main parts of the simulated ecosystem are defined as plant, litter
192 and soil. The most important pools include leaf (C, N and intercepted water), root (C, N),

193 stem (C, N), soil (C, N and water) and litter (C, N). Plant C and N pools have sub-pools
194 (actual pools, storage pools and transfer pools). The actual sub-pools store C and N for the
195 current year growth. The storage sub-pools (essentially the non-structural carbohydrate pool,
196 the source for the cores or buds) contain the amount of C and N that will be active during the
197 next growing season. The transfer sub-pools inherit the entire content of the storage pools at
198 the end of every simulation year. Soil C also has sub-pools representing various organic
199 matter forms characterized by considerably different decomposition rates.

200 In spite of its popularity and proven applicability, the development of Biome-BGC
201 was temporarily stopped (the latest official NTSG version is Biome-BGC 4.2;
202 <https://www.ntsg.umt.edu>). One major drawback of the model was its relatively poor
203 performance in modelling managed ecosystems, and the simplistic soil water balance
204 submodel using a single soil layer only.

205 Our team started to develop the Biome-BGC model further in 2006. According to the
206 logic of the team, the new model branch was planned to be the continuation of the Biome-
207 BGC model with regard to the original concept of the developers (keeping the model code
208 open source, providing detailed documentation, and providing support for the users).

209 The starting point of our model development was Biome-BGC v4.1.1 that was a result
210 of the model improvement activities of the Max Planck Institute (Vetter et al., 2007).
211 Development of the Biome-BGCMuSo model branch has a long history by now. Previous
212 model developments were documented in Hidy et al. (2012) and Hidy et al. (2016). Below,
213 we provide detailed description of the new developments that are included in Biome-
214 BGCMuSo v6.2 which is the latest version released in September, 2021. A comprehensive
215 review of the input data requirement of the model together with explanation on the input data
216 structure is available in the User's Guide (Hidy et al., 2021). In this paper we refer to some
217 input files (e.g. soil file, plant file) that are described in the User's Guide in detail.

218 One of the most important novelty and advantage of the new model version (Biome-
219 BGCMuSo v6.2) compared to any previous versions that due to the extensive and detailed
220 soil parameter set (current version has 79, MuSo 4.0 has 39 and original model version has
221 only 6 adjustable soil related parameters) the parameterization of the model is much more
222 flexible. But this might be of course a challenging task to define all of the input parameters. In
223 order to support practical application of the model, the User's Guide contains proposed values
224 for most of the new parameters (Hidy et al., 2021).

225 **3. Soil hydrology related developments**

226 In Biome-BGCMuSo v6.2 a 10-layer soil submodel was implemented. Previous model
227 versions included a 7-layer submodel, which turned out to be insufficient to capture
228 hydrological events like drying of the topsoil layers with sufficient accuracy. The thicknesses
229 of the layers from the surface to the bottom are 3, 7, 20, 30, 30, 30, 30, 50, 200 and 600 cm.
230 The centre of the given layer represents the depth of each soil layer. Soil texture can be
231 defined by the percentage of sand and silt for each layer separately along with the most
232 important physical and chemical parameters (pH, bulk density, characteristic SWC values,
233 drainage coefficient, hydraulic conductivity) in the soil input file (Hidy et al., 2021).

234 The water balance module of Biome-BGCMuSo has five major components to
235 describe soil water related processes in daily resolution (listed here following the order of
236 calculation): pond water accumulation and runoff; infiltration and downward gravitational
237 flow (percolation); water potential gradient driven water movement within the soil (diffusion);
238 evaporation and transpiration (root water uptake); and the downward/upward fluxes to/from
239 groundwater. In the following subsections these five major components are described.

240 **3.1 Pond water accumulation and runoff**

241 Precipitation can reach the surface as rain or snow (below 0 °C snow accumulation is
242 assumed). Snow water melts from the snowpack as a function of temperature and radiation
243 and added to the precipitation input.

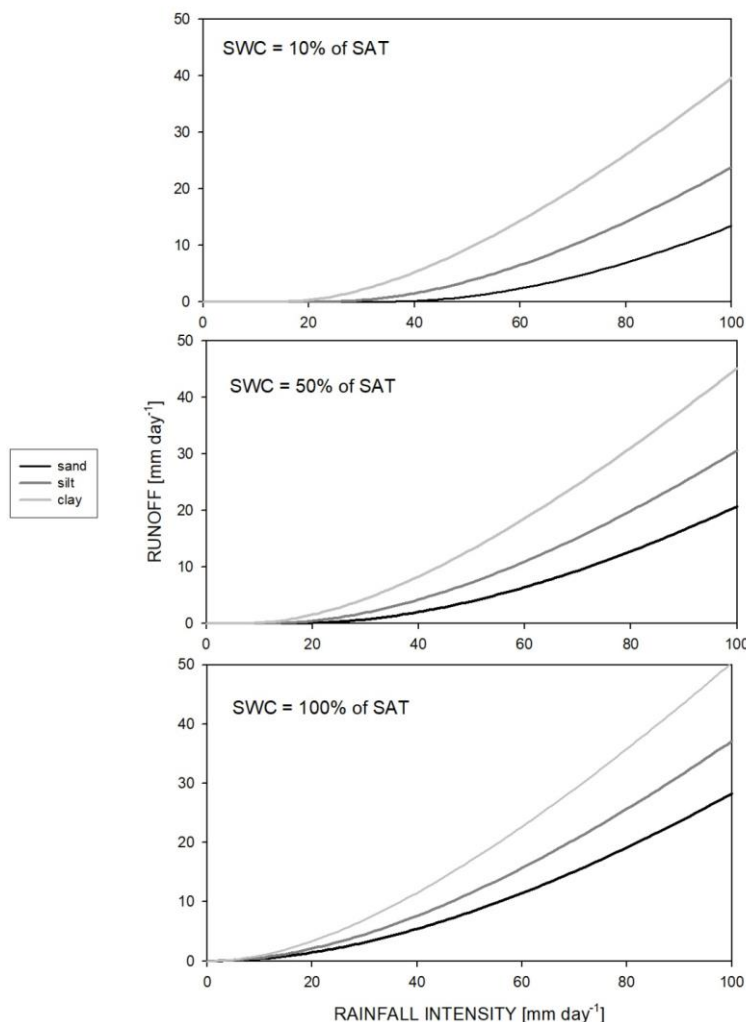
244 The canopy can intercept rain. The intercepted volume goes into the *canopy water*
245 pool, which can evaporate. No canopy interception of snow is assumed. The throughfall
246 (complemented with the amount of melted snow) gives the potential infiltration.

247 A new development in ~~Important novelty of~~ Biome-BGCMuSo v6.2 is that
248 maximum infiltration is calculated based on the saturated hydraulic conductivity and the SWC
249 of the top soil layers. If the potential infiltration exceeds the maximum infiltration, pond water
250 can be formed. If the sum of the precipitation and the actual pond height minus the maximum
251 infiltration rate is greater than the maximum pond height, the excess water is added to surface
252 runoff detailed below (Balsamo et al., 2009). The maximum pond height is an input
253 parameter. Water from the pond can infiltrate into the soil at a rate the top soil layer can
254 absorb it. Evaporation of the pond water is assumed equal to the potential evaporation.

255 Surface runoff is the water flow occurring on the surface when a portion of the
256 precipitation cannot infiltrate into the soil. Two types of surface runoff processes can be

257 distinguished: Hortonian and Dunne. Hortonian runoff is unsaturated overland flow that
258 occurs when the rate of precipitation exceeds the rate at which water can infiltrate. The other
259 type of surface runoff is the Dunne runoff (also known as the saturation overland flow) which
260 occurs when the entire soil is saturated but the rain continues to fall. In this case the rainfall
261 immediately triggers pond water formation and (above the maximum pond water height)
262 surface runoff. The handling of these processes is presented in the soil hydrological module of
263 Biome-BGCMuSo v6.2.

264 Calculation of Hortonian runoff (in $\text{kg H}_2\text{O m}^{-2} \text{ day}^{-1}$) is based on a semi-empirical
265 method and uses the precipitation amount (in cm day^{-1}), the unitless runoff curve number
266 (RCN), and the actual moisture content status of the topsoil (Rawls et al., 1980; this method is
267 known as the SCS runoff curve number method). This type of runoff simulation can be turned
268 off by setting RCN to zero. The detailed description can be found in the Supplementary
269 material, Section 1. The amount of runoff as a function of the soil type and the actual SWC is
270 presented in Figure 1.



271

272 Figure 1: Hortonian runoff as the function of rainfall intensity, soil type and actual soil water content of the top soil
273 layer. Sand soil means 92% sand, 4% silt and 4% clay; silt soil means 8% sand, 86% silt and 6% clay; clay soil means
274 20% sand, 20% silt and 60% clay. SWC and SAT denote~~means~~ soil water content and; SAT ~~means~~ saturation,
275 respectively.

276

277 3.2 Infiltration, percolation and diffusion

278 There are two optional methods in Biome-BGCMuSo v6.2 to calculate soil water
279 movement between soil layers and actual SWC layer by layer. The first one is a cascade
280 method (also known as tipping bucket method), and the second is a Richards equation based
281 physical method. The tipping bucket method has a long history in crop modelling and is
282 considered as a successful, well-evaluated algorithm that can accurately simulate downward
283 water flow in the soil.

284 The cascade method uses a semi-empirical input parameter (DC : drainage coefficient
285 in day^{-1}) to calculate downward water flow rate. When the SWC of a soil layer exceeds field
286 capacity (FC), a fraction (equal to DC) of the water amount above FC goes to the layer next
287 below. If DC is not set in the soil input file, it is estimated from the saturated hydraulic
288 conductivity: $DC = 0.1122 \cdot K_{SAT}^{0.339}$ (K_{SAT} : saturated hydraulic conductivity in cm day^{-1} ;
289 the user can set its value or the model based on soil texture estimates it internally; see Hidy et
290 al., 2016). The detailed description of the method can be found in the Supplementary material,
291 Section 2. Drainage from the bottom layer is a net loss for the soil profile.

292 Water diffusion that is the capillary water flow between the soil layers is calculated to
293 account for the relatively slow movement of water. The flow rate is the function of the water
294 content difference of two adjacent layers and the soil water diffusivity at the boundary of the
295 layers, which is determined based on the average water content of the two layers. The detailed
296 mathematical description of the method can be found in the Supplementary material, Section
297 3.

298 The detailed description of the Richards-~~—~~method can be found in Hidy et al. (2012).
299 To support efficient and robust calculations of soil water fluxes a dynamically changing time
300 step was introduced in version 4.0 (Hidy et al., 2016). ~~An enhancement of this method in~~
301 ~~Biome-BGCMuSo v6.2 is the finer vertical discretisation of the soil profile that is used during~~
302 ~~the numerical solution of the equation.~~ The implementation of the more sophisticated
303 Richards-methodequation is still in an experimental phase requiring rigorous testing and
304 validation in the future.

305 | **3.3 Evapotranspiration**

306 Biome-BGCMuSo, such as its predecessor Biome-BGC, estimates evaporation of leaf
307 intercepted water, bare soil evaporation, and transpiration to estimate the total
308 evapotranspiration in a daily level. The potential rates of all three processes are calculated
309 based on the Penman-Monteith (PM) method. PM equation requires net radiation (minus soil
310 heat flux) and conductance values by definition using different parameterization for the
311 different processes. The model calculates leaf- and canopy-level conductances of water
312 vapour and sensible heat fluxes, to be used in Penman-Monteith calculations of canopy
313 evaporation and canopy transpiration. Note that in the Biome-BGC model family the direct
314 wind effect is ignored but can be considered indirectly by adjusting boundary layer
315 conductance to site-specific conditions. A possible future direction might be the extension of
316 the model logic to consider wind effect directly.

317 | ***3.3.1 Canopy evaporation***

318 If there is intercepted water, this portion of evaporation is calculated using the canopy
319 resistance (reciprocal of conductance) to evaporated water and the resistance to sensible heat.
320 The time required for the water to evaporate based on the average daily conditions is
321 calculated, and subtracted from the day length to get the effective day length for
322 evapotranspiration. Combined resistance to convective and radiative heat transfer is calculated
323 based on canopy conductance of vapour and leaf conductance of sensible heat both of which
324 are assumed to be equal to the boundary layer conductance. Besides the
325 conductance/resistance parameters the canopy absorbed shortwave radiation drives the
326 calculation. Note that the canopy evaporation routine was not modified significantly in
327 Biome-BGCMuSo.

328 | ***3.3.2 Soil evaporation***

329 In order to estimate soil evaporation, first the potential evaporation is calculated,
330 assuming that the resistance to vapour is equal to the resistance to sensible heat and assuming
331 no additional resistance component. Both resistances are assumed to be equal to the actual
332 aerodynamic resistance. Actual aerodynamic resistance is the function of the actual air
333 pressure and air temperature and the potential aerodynamic resistance ($potR_{air}$ in $s m^{-1}$).
334 $potR_{air}$ was a fixed value in the previous model versions ($107 s m^{-1}$). Its value was derived
335 from observations over bare soil in tiger-bush in south-west Niger (Wallace and Holwill,
336 1997). In Biome-BGCMuSo v6.2, the $potR_{air}$ is an input parameter that can be adjusted by the
337 user (Hidy et al., 2021). Another new development in Biome-BGCMuSo v6.2 is the

338 introduction of an upper limit for daily potential evaporation ($evap_{limit}$) that is determined by
339 the available energy (incident shortwave flux that reaches the soil surface):

340
$$evap_{limit} = \frac{irad \cdot dayl}{LH_{vap}} \quad (1)$$

341 where $irad$ is the incident shortwave flux density in W m^{-2} , $dayl$ is the length of the day in
342 seconds, LH_{vap} is the latent heat of vaporization (the amount of energy that must be added to
343 liquid to transform into gas) in J kg^{-1} . This feature was missing from previous model versions
344 resulting in considerable overestimation of evaporation on certain days that was caused by the
345 missing energy limitation on evaporation.

346 **A new feature** **An important novelty** in Biome-BGCMuSo v6.2 is the calculation of
347 the actual evaporation from the potential evaporation and the square root of time elapsed since
348 the last precipitation (expressed by days; Ritchie, 1998). This is another method that has been
349 used by the crop modeller community for many years. Detailed description of the algorithm
350 can be found in the Supplementary material, Section 4.

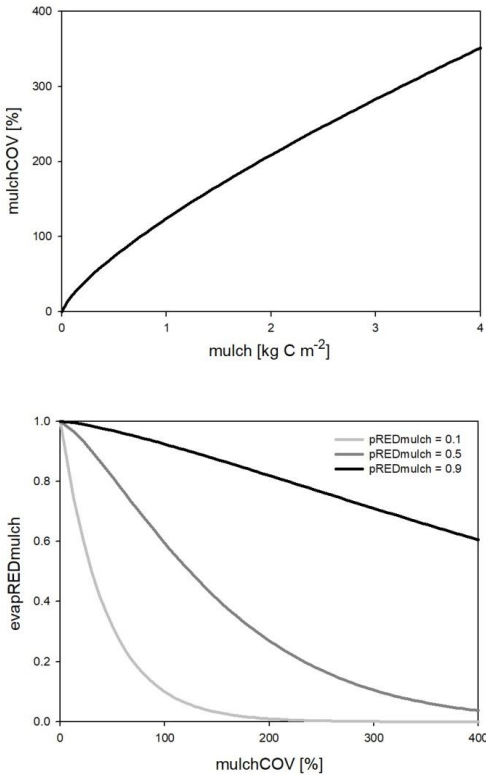
351 **One** **A** major **new development** **novel feature** in Biome-BGCMuSo v6.2 is the
352 simulation of the reducing effect of surface residue or mulch cover on bare soil evaporation.
353 Here we use the term ‘mulch’ to quantify surface residue cover in general keeping in mind
354 that mulch is typically a human-induced coverage. Surface residue includes aboveground
355 litter and coarse woody debris as well.

356 The evaporation reduction effect ($evapREDmulch$; unitless) is a variable between 0
357 and 1 (0 means full limitation, and 1 means no limitation) estimated based on a power
358 function of the surface coverage ($mulchCOV$ in %) and a soil specific constant set by the user
359 ($pREDmulch$; see Hidy et al., 2021). If variable $mulchCOV$ reaches 100% it means that the
360 surface is completely covered. If $mulchCOV$ is greater than 100% it means the surface is
361 covered by more than one layers. Surface coverage is a power function of the amount of
362 mulch (mu in kgC m^{-2}) with parameters $p1_{mulch}$, $p2_{mulch}$, and $p3_{mulch}$ (soil parameters) based
363 on the method of Rawls et al. (1991):

364
365
$$mulchCOV = p1_{mulch} \cdot (mu / p2_{mulch})^{p3_{mulch}} \quad (2)$$

366
$$evapREDmulch = pREDmulch^{\frac{mulchCOV}{100}} \quad (3)$$

367 Another simulated effect of surface residue cover is the homogenization of soil
368 temperature between 0 and 30 cm depth (layers 1, 2 and 3). The functional forms of surface
369 coverage and evaporation reduction factor are presented in Figure 2.



370

371 **Figure 2: Surface coverage as a function of the amount of surface residue or mulch (upper plot)** and the evaporation
 372 **reduction factor (evapREDmulch) as the function of mulch coverage (lower plot) using different mulch specific soil**
 373 **parameters (pREDmulch). See text for details.**

374

375 3.3.3 Transpiration

376 In order to simulate transpiration, first transpiration demand (TD in $\text{kg H}_2\text{O m}^{-2} \text{ day}^{-1}$)
 377 is calculated using the Penman-Monteith equation separately for sunlit and shaded leaves. TD
 378 is the function of leaf-scale conductance to water vapor, which is derived from stomatal,
 379 cuticular and leaf boundary layer conductances. A novelty in Biome-BGCMuSo v6.2 is that
 380 potential evapotranspiration is also calculated using the maximal stomatal conductance
 381 instead of the actual stomatal conductance, which means that stomatal aperture is not affected
 382 by the soil moisture status (in contrast to the actual one).

383 TD is distributed across the soil layers according to the actual root distribution using
 384 an improved method (the logic was changed since Biome-BGCMuSo v4.0). From the plant
 385 specific root parameters and the actual root weight Biome-BGCMuSo calculates the number
 386 of the layers where roots can be found together with the root mass distribution across the
 387 layers (Jarvis, 1989; Hidy et al., 2016).- If there is not enough water in a given soil layer to
 388 fulfil the transpiration demand, the transpiration flux from that layer is limited, and below
 389 wilting point (WP) it is set to zero. The sum of layer-specific transpiration fluxes across the

390 root zone gives the actual transpiration flux. The detailed description of the algorithm can be
391 found in the Supplementary material, Section 5.

392 **3.4 Effect of groundwater**

393 Simulation of groundwater effect was introduced in Biome-BGCMuSo v4.0 (Hidy et
394 al., 2016), but the method has been significantly improved, and the new algorithm it is now
395 available in Biome-BGCMuSo v6.2. In the recent model version there is an option to provide
396 an additional input file with the daily values of the groundwater table depth (*GWdepth* in m).

397 Groundwater may affect soil hydrological and plant physiological processes if the
398 water table is closer to the root zone than the thickness of the capillary fringe (that is the
399 region saturated from groundwater via capillary effect). The thickness of the capillary fringe
400 (*CF* in m) is estimated using literature data and depends on the soil type (Johnson and Ettinger
401 model; Tillman and Weaver, 2006). Groundwater table distance (*GWdist* in m) for a given
402 layer is defined as the difference between *GWdepth* and the depth of the midpoint of the
403 layer.

404 The layers completely below the groundwater table are assumed to be fully saturated.
405 In case of layers within the capillary fringe (*GWdist* < *CF*), the calculation of water balance
406 changes: the ~~FC~~**field capacity** rises, thus the difference between saturation (SAT) and FC
407 decreases and the layer charges gradually, till the increased FC value is reached. The FC-
408 rising effect of groundwater for the layers above the water table is calculated based on the
409 ratio of the groundwater distance and the capillary fringe thickness, but only after the water
410 content of the layers below have reached their modified FC values. Detailed description of the
411 groundwater effect can be found in Supplementary material, Section 6.

412 **3.5 Soil moisture stress**

413 In the original Biome-BGC model the effect of changing soil water content on
414 photosynthesis and decomposition of soil organic matter is expressed in terms of soil water
415 potential (Ψ). Instead of Ψ , the ~~volumetric~~ SWC is also widely used to calculate the limitation
416 of stomatal conductance and decomposition. A practical advantage of using SWC as a factor
417 in stress function is that it is easier to measure in the field and the changes of the driving
418 function are much smoother than in case of Ψ . The disadvantage is that SWC is not
419 comparable among different soil types (in contrast to Ψ).

420 The maximum of SWC is the saturation value; the minimum is the wilting point or the
421 hygroscopic water depending on the type of the simulated process. Novelty of Biome-

422 BGCMuSo v6.2 is that the hygroscopic water, the wilting point, the field capacity and the
 423 saturation values are calculated internally by the model based on the soil texture data, or can
 424 be defined in the input file layer by layer.

425 In Biome-BGCMuSo v6.2 the so-called soil moisture stress index (*SMSI*) is calculated
 426 to represent overall soil stress conditions. *SMSI* is affected by the length of the drought event
 427 (*SMSE*: extent of soil stress), the severity of the drought event (*SMSL*: length of soil stress),
 428 aggravated by the extreme temperature (*extremT*: effect of extreme heat). *SMSI* is equal to
 429 zero if no soil moisture limitation occurs and equal to 1 in case of full soil moisture limitation.
 430 *SMSI* is used by the model for plant senescence calculations (presentation of plant related
 431 processes is the subject of a forthcoming publication)). The members of *SMSI* are explained
 432 detailed below.

433 |

434
$$SMSI = 1 - SMSE \cdot SMSL \cdot extremT \quad (4)$$

435 Magnitude of soil moisture stress (*SMSE*) is calculated layer by layer based on SWC.
 436 Regarding soil moisture stress two different processes are distinguished: drought (i.e. low
 437 SWC close to or below WP) and anoxic condition (i.e. after large precipitation events or in
 438 the presence of high groundwater table; Bond-Lamberty et al., 2007). An important novelty of
 439 Biome-BGCMuSo v6.2 is the soil curvature parameters (*q*) which is introduced to provide
 440 mechanism for soil texture dependent drought stress as it can affect the shape of the soil stress
 441 function (which means possibility for non-linear ramp function):

442 |

443
$$SMSE^i = 0 \quad ; SWC^i < SWC_{WP}^i$$

444
$$SMSE^i = \left(\frac{SWC^i - SWC_{WP}^i}{SWC_{drought}^i - SWC_{WP}^i} \right)^q \quad ; SWC_{WP}^i \leq SWC^i < SWC_{drought}^i \quad (5)$$

445
$$SMSE^i = 1 \quad ; SWC_{drought}^i \leq SWC^i \leq SWC_{anoxic}^i$$

446
$$SMSE^i = \frac{SWC_{SAT}^i - SWC^i}{SWC_{SAT}^i - SWC_{anoxic}^i} \quad ; SWC^i > SWC_{anoxic}^i$$

447 where *q* is the curvature of soil stress function, $SWC_{drought}^i$ and SWC_{anoxic}^i are critical SWC
 448 values for calculating soil stress.

449 In order to make the SWC values comparable between different soil types,
 450 $SWC_{drought}^i$ and SWC_{anoxic}^i can be set in normalized form (such as in Eq. 4) as part of the
 451 ecophysiological parameterization of the model. More details about the adjustment of the
 452 critical SWC values can be found in Hidy et al. (2021).

453 The layer specific soil moisture stress extent values are summed across the root zone
 454 using the relative amount of roots in the layers (RP^j) as weighting factors to obtain the overall
 455 soil moisture stress extent ($SMSE$):

$$456 \quad SMSE = \sum_{i=0}^{i=nr} SMSE^i \cdot RP^i \quad (6)$$

$$457 \quad RP^i = RD \frac{z^i}{RL} \cdot e^{-RD \cdot (mid^i / RL)} \quad (7)$$

458 where nr is the number of the soil layers where roots can be found, RL is the actual length of
 459 roots, RD is rooting distribution parameter (ecophysiological parameter; see details in the
 460 User's Guide; Hidy et al., 2021). In the current model version $SMSE$ can also affect the entire
 461 photosynthetic machinery by the introduction of an empirical parameter. This mechanism is
 462 responsible to account for the non-stomatal effect of drought on photosynthesis (details about
 463 this algorithm will be published in a separate paper). Since there is no mechanistic
 464 representation behind this empirical down-regulation of photosynthesis, further test are
 465 needed for the correct setting of this parameter using preferentially eddy covariance data.

The soil moisture stress length related factor (*SMSL*) is the ratio of the critical soil moisture stress length (ecophysiological parameter) and the sum of the daily ($1 - SMSE$) values. This cumulated value restarts if *SMSE* is equal to one (no stress). Extreme heat (*extremT*) is also considered and is taken into account in the final stress function (see above) by using a ramp function. Its parameterization thus requires the setting of two critical temperature limits that defines the ramp function (set by the ecophysiological parameterization; see Hidy et al., 2021). Its characteristic temperature values can be set by parameterization (ecophysiological input file).

474 4. Soil carbon and nitrogen cycles

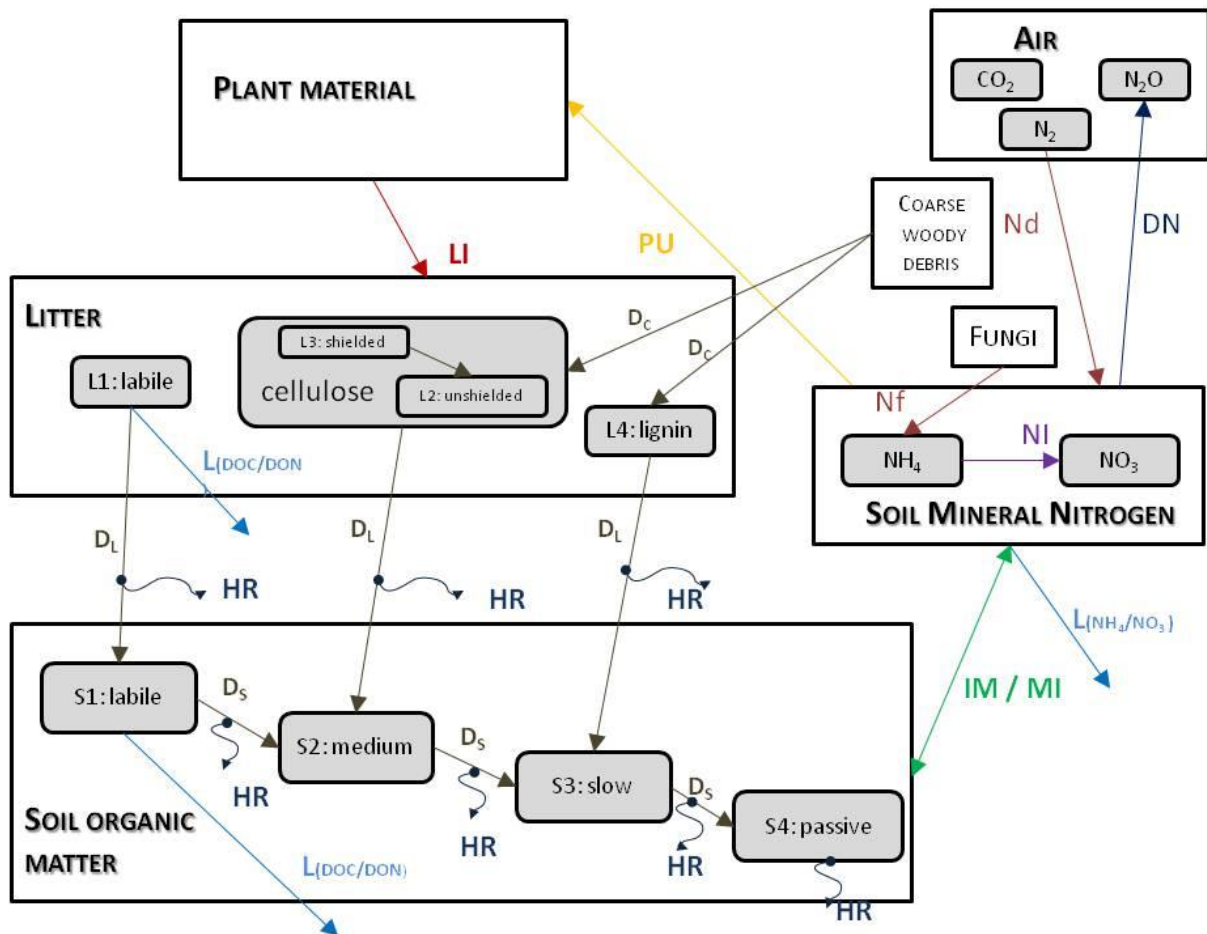
475 4.1 Soil-litter module

476 We made substantial changes in the soil biogeochemistry module of the Biome-BGC
477 model. Previous model versions already offered solutions for multilayer simulations (Hidy et
478 al., 2012, 2016), but some pools still inherited the single-layer logic of the original model. In
479 the new model version all relevant soil processes are separated layer by layer which is a major
480 step forward.

Instead of defining a single litter, soil organic carbon (SOC) and nitrogen pool, we implemented separate carbon and nitrogen pools for each soil layer in the form of soil organic matter (SOM) and litter in Biome-BGCMuSo v6.2. The changes of the mass of the carbon and

484 nitrogen pools are calculated layer by layer. Mortality fluxes (whole plant mortality,
485 senescence, litterfall) of aboveground plant material are transferred into the litter pools of the
486 top soil layers (0-10 cm, layers 1-2). Mortality fluxes of belowground plant material are
487 transferred into the corresponding soil layers based on their location within the root zone. Due
488 to ploughing and leaching, carbon and nitrogen can also be relocated to deeper layers. The
489 plant material turning into the litter compartment is divided between the different types of
490 litter pools (labile, unshielded cellulose, shielded cellulose and lignin) according to the
491 parameterization. Litter and soil decomposition fluxes (carbon and nitrogen fluxes from litter
492 to soil pools) are calculated layer by layer, depending on the actual temperature and SWC of
493 the corresponding layers. Vertical mixing of soil organic matter between the soil layers (e.g.
494 bioturbation) is not implemented in the current model version.

495 Figure 3 shows the most important simulated soil and litter processes. N-fixation (N_f)
496 is the N input from the atmosphere to soil layers in the root zone by microorganisms. The user
497 can set its annual value as an input parameter. N-deposition (N_d) is the N input from the
498 atmosphere to the top soil layers (see below). The user can set its annual value as a site-
499 specific parameter in the initialization input file. Nitrogen deposition can be provided by
500 annually varying values as well. Plant uptake (P_U) is the absorption of mineral N by plants
501 from the soil layers in the root zone. Mineralization (M_l) is the release of plant-available
502 nitrogen (flux from soil organic matter to mineralized nitrogen). Immobilization (I_M) is the
503 consumption of inorganic nitrogen by microorganisms (flux from mineralized nitrogen to soil
504 organic matter). Nitrification (N_l) is the biological oxidation of ammonium to nitrate through
505 nitrifying bacteria. Denitrification (D_N) is a microbial process where nitrate (NO_3^-) is reduced
506 and converted to nitrogen gas (N_2) through intermediate nitrogen oxide gases. Leaching (L) is
507 the loss of water-soluble mineral nitrogen from the soil layers. If leaching occurs in the
508 lowermost soil layer that means loss of N from the simulated system. Litterfall (L_f) is the
509 plant material transfer from plant compartments to litter. Decomposition is the C and N
510 transfer from litter to soil pools and between soil pools. In case of woody vegetation coarse
511 woody debris (CWD) contains the woody plant material after litterfall before physical
512 fragmentation. Litter has also four sub-pools based on their composition: labile (L1),
513 unshielded and shielded cellulose (L2, L3) and lignin (L4). Soil organic matter has also four
514 sub-pools based on their turnover rate: labile (S1), medium (S2), slow (S3) and passive
515 (recalcitrant; S4) SOM pool. Soil mineralized nitrogen pool contains the inorganic N-forms of
516 the soil: ammonium and nitrate.



517

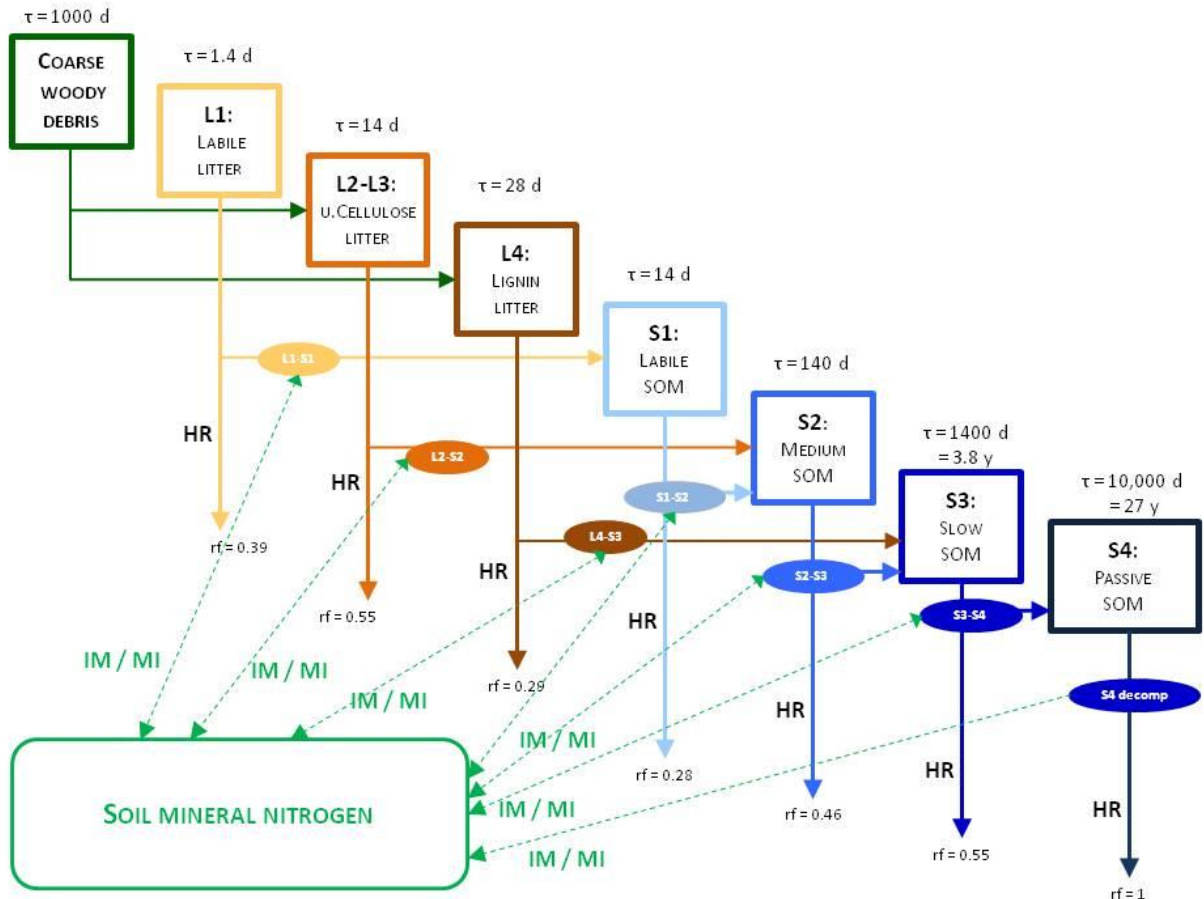
518 Figure 3: Soil and litter related simulated carbon/nitrogen fluxes (arrows) and pools (rectangles) in Biome-BGCMuSo
 519 v6.2. HR: heterotrophic respiration, IM: immobilization, MI: mineralization, PU: plant uptake, LI: litterfall, NI:
 520 nitrification, D: decomposition (D_L : decomposition of litter, D_S : decomposition of SOM, D_C : fragmentation of coarse
 521 woody debris), L: leaching, Nf: nitrogen fixation, Nd: nitrogen deposition, DN: denitrification. L represents loss of C
 522 and N from the simulated system.

523

524 4.2 Decomposition

525 In the decomposition module (i.e. converging cascade scheme; Thornton, 1998) the
 526 fluxes between litter and soil pools are calculated layer by layer. The potential fluxes are
 527 modified in case of N limitation when the potential gross immobilization is greater than the
 528 potential gross mineralization.

529 To explain the decomposition processes implemented in Biome-BGCMuSo v6.2 the
 530 main carbon/nitrogen pools and fluxes between litter and soil organic and inorganic
 531 (mineralized) matter are presented on Figure 4.



532

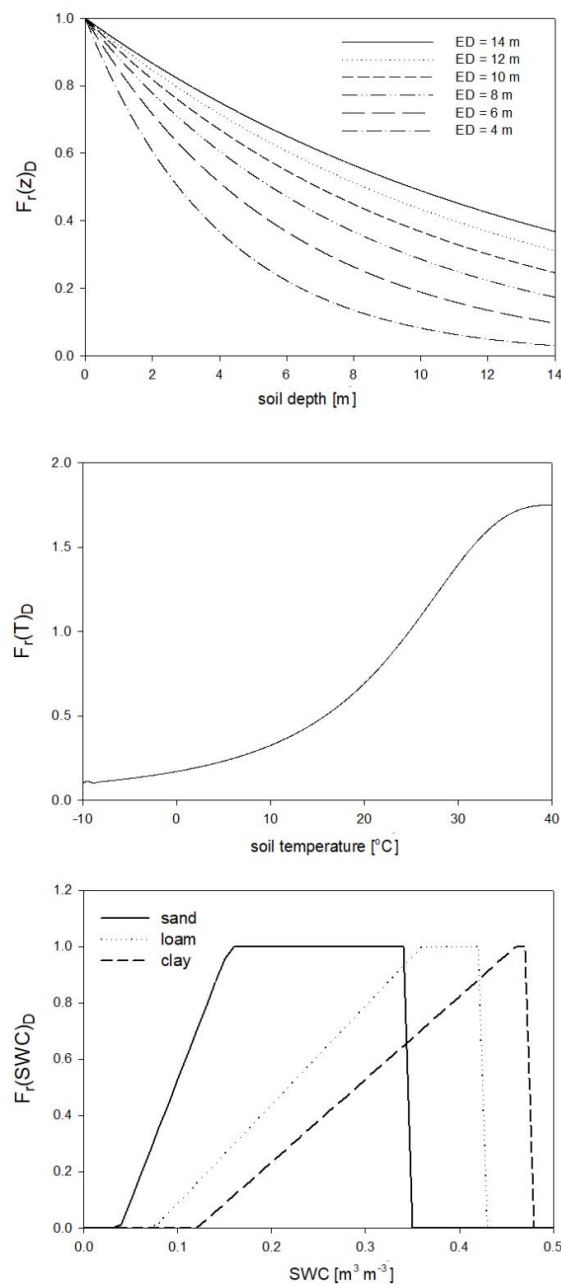
533 Figure 4: Overview of the converging cascade model of litter and soil organic matter decomposition that is
 534 implemented in Biome-BGCMuSo v6.2. rf represents the respiration fraction of the different transformation fluxes, τ
 535 is the residence time (reciprocal of the rate constants that is the turnover rate), IM/MI: immobilization
 536 and mineralization fluxes, HR: heterotrophic respiration. Note that both the respiration fraction and the turnover rate parameters can be
 537 adjusted through parameterization.

538

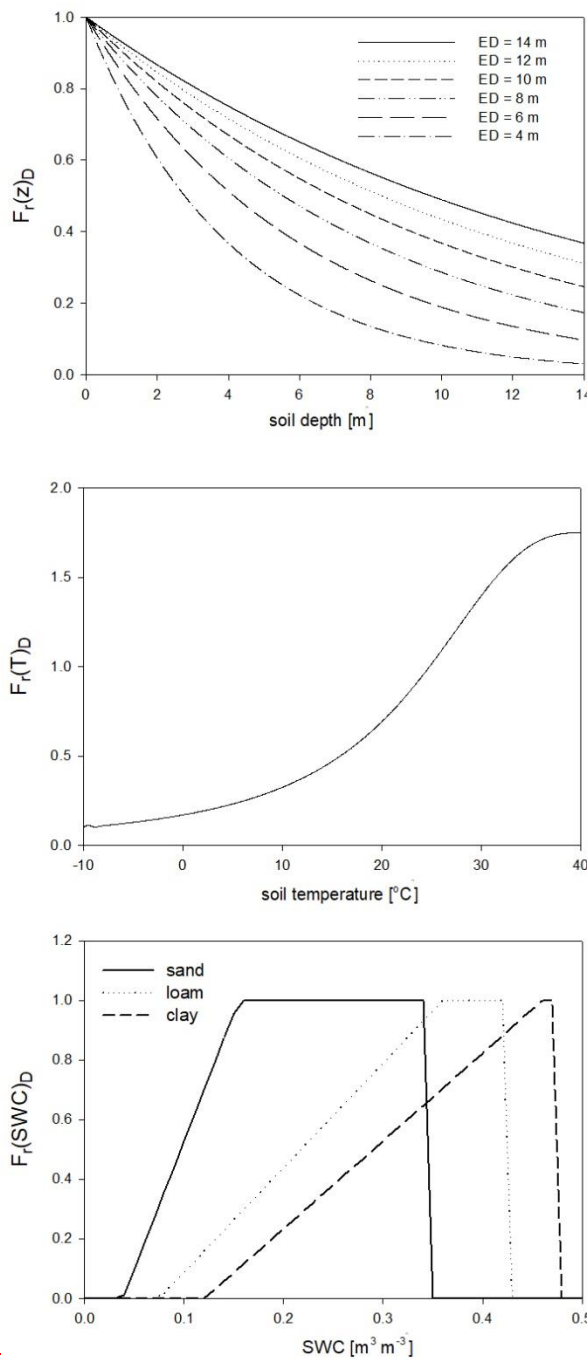
539 In the original Biome-BGC and in previous Biome-BGCMuSo versions the C:N ratio
 540 (CN) of the soil pools were fixed in the model code. One of the new features in
 541 Biome-BGCMuSo v6.2 is that the CN of the passive soil pool (S4 in Figure 4; recalcitrant soil
 542 organic matter) can be set by the user as a soil parameter. The CN of the other soil pools
 543 (labile, medium and slow; S1, S2 and S3) are calculated based on the proportion of fixed CN
 544 values of the original Biome-BGC ($CN_{labile}/CN_{passive} = 1.2$, $CN_{medium}/CN_{passive} = 1.2$, $CN_{slow}/$
 545 $CN_{passive} = 1$). Note that the CN of the donor and acceptor pools are used in decomposition
 546 calculations (see details in Supplement Material, Section 7), and as a result these parameters
 547 set the C:N ratio of the soil pools. The donor and acceptor pools can be seen in Figure 3 and
 548 Figure 4.

549 For the calculation of nitrogen mineralization first respiration cost (respiration
 550 fraction) is estimated. Mineralization then is the function of the remaining part of the pool

551 and its C:N ratio. The nitrogen mineralization fluxes of the SOM pools are functions of the
 552 potential rate constant (reciprocal of residence time), and the integrated response function that
 553 accounts for the impact of multiple environmental factors. The integrated response function of
 554 decomposition is a product of the response functions of depth, soil temperature and SWC
 555 ($F_r(d)_D$, $F_r(T)_D$, $F_r(SWC)_D$; Figure 5). Its detailed description can be found in the
 556 Supplementary material, Section 7. The dependence of the three different factors on depth,
 557 temperature and SWC with default parameters are presented in Figure 5.



558



559

560 Figure 5: The dependence of the individual factors that form the complex environmental response function of
 561 decomposition on depth ($F_r(d)_D$), temperature ($F_r(T)_D$) and SWC in case of different soil types ($F_r(SWC)_D$). ED is the
 562 e-folding depth which is one of the adjustable soil parameters of the model. [For the definition of sand, silt and clay see](#)
 563 [Figure 1](#)
 564 [Sand-soil means 92% sand, 4% silt and 4% clay; silt-soil means 8% sand, 86% silt and 6% clay; clay-soil
 means 20% sand, 20% silt and 60% clay.](#)

565

566 4.3 Soil nitrogen processes

567 In Biome-BGCMuSo v6.2 separate ammonium ($sNH4$) and nitrate ($sNO3$) soil pools
 568 are implemented instead of a general mineralized nitrogen pool. This was a necessary step for

569 the realistic representation of many internal processes like plant nitrogen uptake, nitrification,
570 denitrification, consideration of the effect of different mineral and organic fertilizers and N_2O
571 emission.

572 It is important to introduce the *availability* concept that Biome-BGCMuSo uses and is
573 associated with the ammonium and nitrate pools. We use the logic proposed by Thomas et al.
574 (2013) which means that the plant has access only to a part of the given inorganic nitrogen
575 pool. Unavailable part is buffered as it is associated with soil aggregates and is unavailable for
576 plant uptake. The available part of ammonium is calculated based on *NH₄ mobilen proportion*
577 (that is a soil parameter set to 10% according to Thomas et al., 2013; Hidy et al., 2021) and
578 the actual pool. The available part of nitrate is assumed to be 100%.

579 The amount of ammonium and nitrate are determined layer by layer controlled by
580 input and output fluxes (F in $\text{kg N m}^{-2} \text{ day}^{-1}$) listed below:

$$581 F_{\text{SNH}_4}^i = IN_{\text{SNH}_4}^i - L_{\text{SNH}_4}^i + L_{\text{SNH}_4}^{i-1} - PU_{\text{SNH}_4}^i - IM_{\text{SNH}_4}^i + MI_{\text{SNH}_4}^i - NI_{\text{SNH}_4}^i \quad (8)$$

$$582 F_{\text{SNO}_3}^i = IN_{\text{SNO}_3}^i - L_{\text{SNO}_3}^i + L_{\text{SNO}_3}^{i-1} - PU_{\text{SNO}_3}^i - IM_{\text{SNO}_3}^i + MI_{\text{SNO}_3}^i - DN_{\text{SNO}_3}^i \quad (9)$$

583 where $IN_{\text{SNH}_4}^i$ and $IN_{\text{SNO}_3}^i$ are the input fluxes to the ammonium and nitrate pools, respectively;
584 $L_{\text{SNH}_4}^i$, $L_{\text{SNH}_4}^{i-1}$, $L_{\text{SNO}_3}^i$, $L_{\text{SNO}_3}^{i-1}$ are the amount of leached mineralized ammonium and nitrate from
585 a layer (i) or from the upper layer ($i-1$), respectively; $PU_{\text{SNH}_4}^i$ and $PU_{\text{SNO}_3}^i$ are the plant uptake
586 fluxes of ammonium and nitrate, respectively; $IM_{\text{SNH}_4}^i$ and $IM_{\text{SNO}_3}^i$ are the immobilization
587 fluxes of ammonium and nitrate, respectively; $MI_{\text{SNH}_4}^i$ and $MI_{\text{SNO}_3}^i$ are the mineralization
588 fluxes of ammonium and nitrate, respectively; $NI_{\text{SNH}_4}^i$ is the nitrification flux of ammonium
589 and $DN_{\text{SNO}_3}^i$ is the denitrification flux of nitrate.

590 In the following subsections the different terms of the equations are described in
591 detail.

592 Input to the sNH₄ and sNO₃ pools (IN in Eq. 6 and 7)

593 According to the model logic N-fixation occurs in the root zone layers. Its distribution
594 between sNH₄ and sNO₃ pools is calculated based on their actual available proportion in the
595 actual layer ($NH4prop^i$):

$$596 NH4prop^i = sNH4avail^i + sNO3avail^i \quad (10)$$

597 where $sNH4avail^i$ and $sNO3avail^i$ are the available part of the sNH₄ and sNO₃ pools in the
598 actual layer.

599 N-deposition related nitrogen input is associated with the 0-10 cm soil layers assuming
600 uniform distribution across layers 1-2 in the model, and the distribution between sNH₄ and

601 sNO₃ pools is calculated based on the *proportion of NH₄ flux of N-deposition* soil parameter
602 (Hidy et al., 2021).

603 Organic and inorganic fertilization is also an optional nitrogen input. The amount and
604 composition (NH₄⁺ and NO₃⁻ content) can be set in the fertilization input file.

605

606 Leaching - downward movement of mineralized N (L in Eq. 6 and 7)

607 The amount of leached mineralized N (mobile part of the given N pool) from a layer is
608 directly proportional to the amount of drainage and the available part of the sNH₄ and sNO₃
609 pools. Leaching from the layer above is a net gain, while leaching from actual layer is a net
610 loss for the actual layer. Leaching is described in Section 4.5.

611

612 Plant uptake by roots (PU in Eq. 6 and 7)

613 N uptake required for plant growth is estimated in the photosynthesis calculations and
614 the amount is distributed across the layers in the root zone. The partition of the N uptake
615 between sNH₄ and sNO₃ pools is calculated based on their actual available proportion in each
616 layer.

617

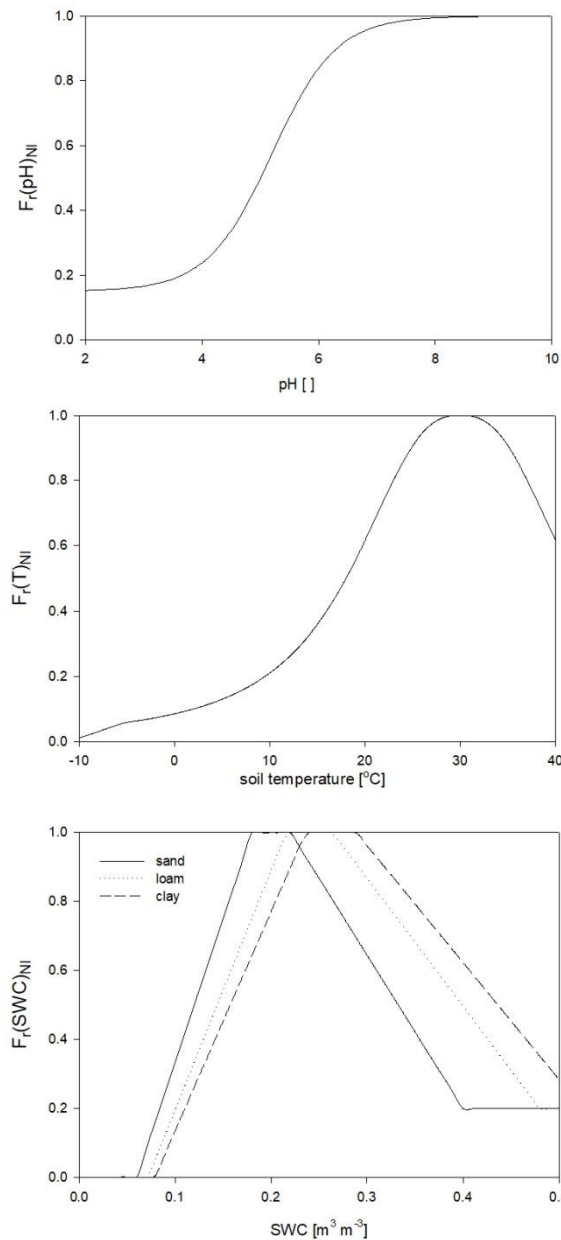
618 Mineralization and immobilization (MI and IM Eq. 6 and 7)

619 Mineralization and immobilization calculations are detailed in Section 4.2. The
620 distribution of these N fluxes between sNH₄ and sNO₃ pools is calculated based on their
621 actual available proportion in each layer.

622

623 Nitrification (NI Eq. 6 and 7)

624 Nitrification is a function of the soil ammonium content, the net mineralization and the
625 response functions of temperature, soil pH and SWC ($F_r(pH)_{NI}$, $F_r(T)_{NI}$, and $F_r(SWC)_{NI}$,
626 respectively) based on the method of Parton et al. (2001) and Thomas et al. (2013). Its
627 detailed mathematical description can be found in the Supplementary material, Section 8. The
628 response functions with proposed parameters are shown in Figure 6.



629

630 **Figure 6: The dependence of the individual factors of the environmental response function of nitrification on soil pH**
 631 **($F_r(pH)_{NI}$), temperature ($F_r(T)_{NI}$) and SWC $F_r(SWC)_{NI}$ in case of different soil types. pH and temperature response**
 632 **functions are independent of the soil texture.**

633

634 Denitrification (DN Eq. 6 and 7)

635 Denitrification flux is estimated with a simple formula (Thomas et al., 2013):

636
$$DN^i = DNcoeff \cdot SOMresp^i \cdot sNO3avail^i \cdot WFPS^i \quad (11)$$

637 where DN of the actual layer is the product of the available nitrate content ($sNO3avail$ in
 638 kg N m^{-2}), $SOMresp^i$ in $\text{g C m}^{-2} \text{ day}^{-1}$ is the SOM decomposition related respiration cost, the
 639 $WFPS^i$ is the water-filled pore space and $DNcoeff$ is the *soil respiration related*
 640 *denitrification rate* in g C^{-1} , which is an input soil parameter (Hidy et al., 2021). The unitless

641 water-filled pore space is the ratio of the actual and the saturated SWC. SOM decomposition
642 associated respiration is the sum of the heterotrophic respiration fluxes of the four soil
643 compartments (S1-S4, Figure 4.).

644 |

645 **4.4 N₂O-emission and N-emission**

646 | —

647 During both nitrification and denitrification N₂O-emission occurs which (added to the
648 N₂O-flux originated from grazing processes if applicable) contributes to the total N₂O-
649 emission of the examined ecosystem.

650 In Biome-BGCMuSo v6.2 a fixed part (set by the *coefficient of N₂O emission of*
651 *nitrification* input soil parameter; Hidy et al., 2021) of nitrification flux is lost as N₂O and not
652 converted to NO₃.

653 During denitrification, nitrate is transformed into N₂ and N₂O gas depending on the
654 environmental conditions: NO₃ availability, total soil respiration (proxy for microbial
655 activity), SWC and pH. The *denitrification related N₂/N₂O ratio* input soil parameter is used
656 to represent the effect of the soil type on the N₂/N₂O ratio (del Grosso et al., 2000; Hidy et al.,
657 2021). Detailed mathematical description of the algorithm can be found in the Supplementary
658 material, Section 9.

659 |

660 **4.5 Leaching of dissolved matter**

661 Leaching of nitrate, ammonium, and dissolved organic carbon and nitrogen (DOC and
662 DON) content from the actual layer is calculated as the product of the concentration of the
663 dissolved component in the soil water and the amount of water (drainage plus diffusion)
664 leaving the given layer either downward or upward. The dissolved component (concentration)
665 of organic carbon is calculated from the SOC pool contents and the corresponding *fraction of*
666 *dissolved part of SOC* soil parameters. The dissolved component of organic nitrogen content
667 of the given soil pool is calculated from the carbon content and the corresponding C:N ratio.
668 The downward leaching is net loss from the actual layer and net gain for the layer next below;
669 the upward flux is net loss for the actual layer and net gain for the layer next up. The
670 downward leaching of the bottom active layer (9th) is net loss for the system. The upward
671 movement of dissolved substance from the passive (10th) layer is net gain for the system.

672 **5. Case studies**

673 **5.1 Evaluation of soil hydrological simulation**

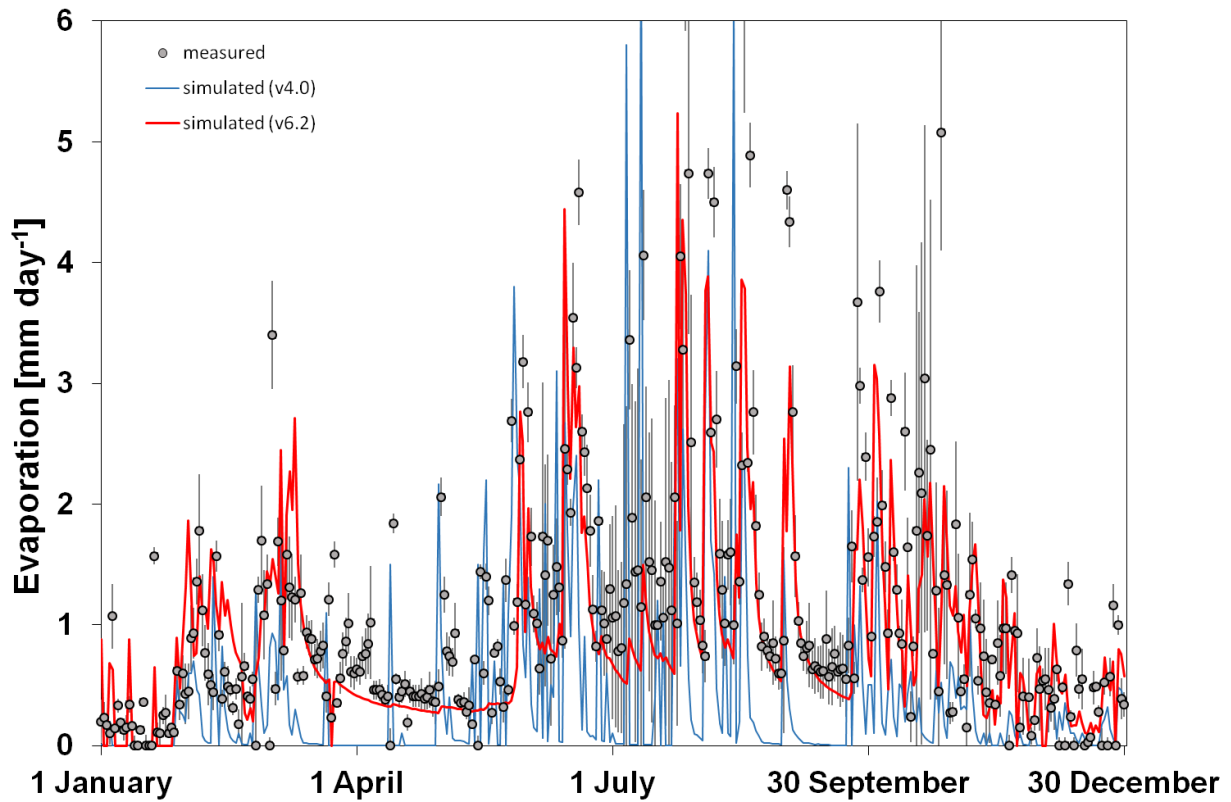
674 In order to evaluate the functioning of the new model version (and to compare
675 simulation results made by the current and the previously published model version), a case
676 study is presented regarding soil water content and soil evaporation simulations. The results
677 of a bare soil simulation (i.e. no plant is assumed to be present) are compared to observation
678 data of a weighing lysimeter station installed at Martonvásár, Hungary (47°18'57.6"N,
679 18°47'25.6"E) in 2017. The climate of the area is continental with a 30-year average
680 temperature of 11.0 °C (–1 °C in January and 21.2 °C in July) and annual rainfall of 548 mm,
681 based on data of the on-site weather station.

682 The station consists of twelve 2 meter deep scientific lysimeter columns with 1 m
683 diameter (Meter Group Inc., USA) with soil temperature, SWC and soil water potential
684 sensors installed at 5, 10, 30, 50, 70, 100 and 150 cm depth. Observation data for 2020 from
685 six columns without vegetation cover (i.e. bare soil) was used to validate the model.

686 Raw lysimeter observation data were processed using standard methods. Bare soil
687 evaporation values were derived— based on changes of the mass of the soil columns also
688 considering the mass change of the drainage water. Additionally, experience has shown that
689 wind speed is related to the high frequency mass change of the soil column mass. To reduce
690 noise, 5-point (5-min) moving averages were used based on Marek et al. (2014). After quality
691 control of the data, the corrected and smoothed lysimeter mass values were used for the
692 calculations. SWC observations were averaged to daily resolution to match the time step of
693 the model.

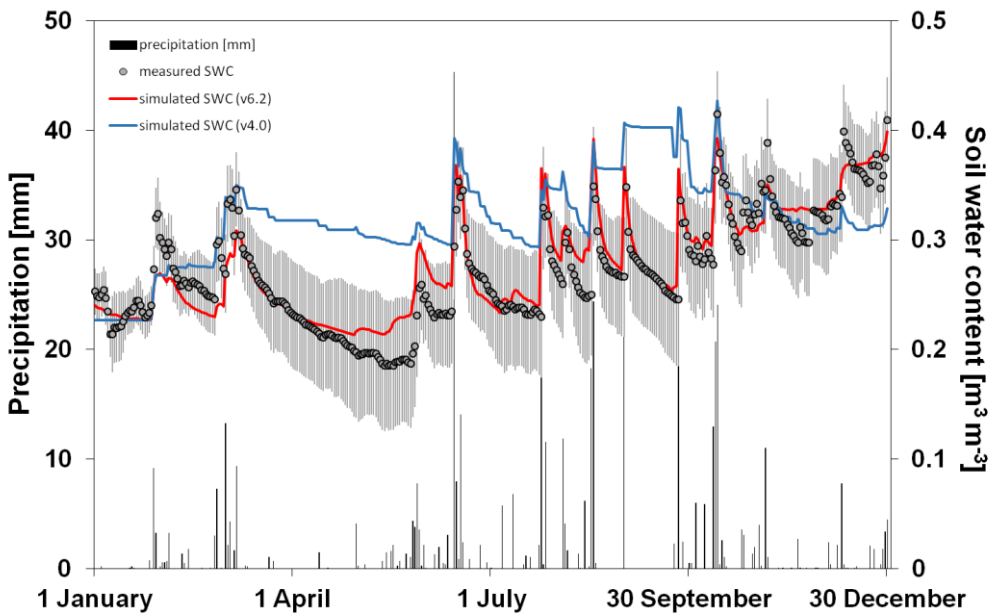
694 Observed local meteorology was used to drive the models for year 2020. Soil physical
695 model input parameters (field capacity, wilting point, bulk density, etc.) were determined in
696 the laboratory using 100 cm³ undisturbed soil samples taken from various depths during the
697 installation of the lysimeter station. Regarding other soil parameters the proposed values were
698 used. Detailed description of the input soil parameters and their proposed values are presented
699 in the User's Guide (Hidy et al., 2021).

700 In Figure 7 the simulated and the observed time series of soil evaporation are
701 presented for Martonvásár, for 2020. The figure shows that the soil evaporation simulation by
702 v6.2 is more realistic than by v4.0. Biome-BGCMuSo v4.0 provides very low values during
703 summer in some days which is not in accordance with the observations. Biome-BGCMuSo
704 v6.2 provides more realistic values during this time period.

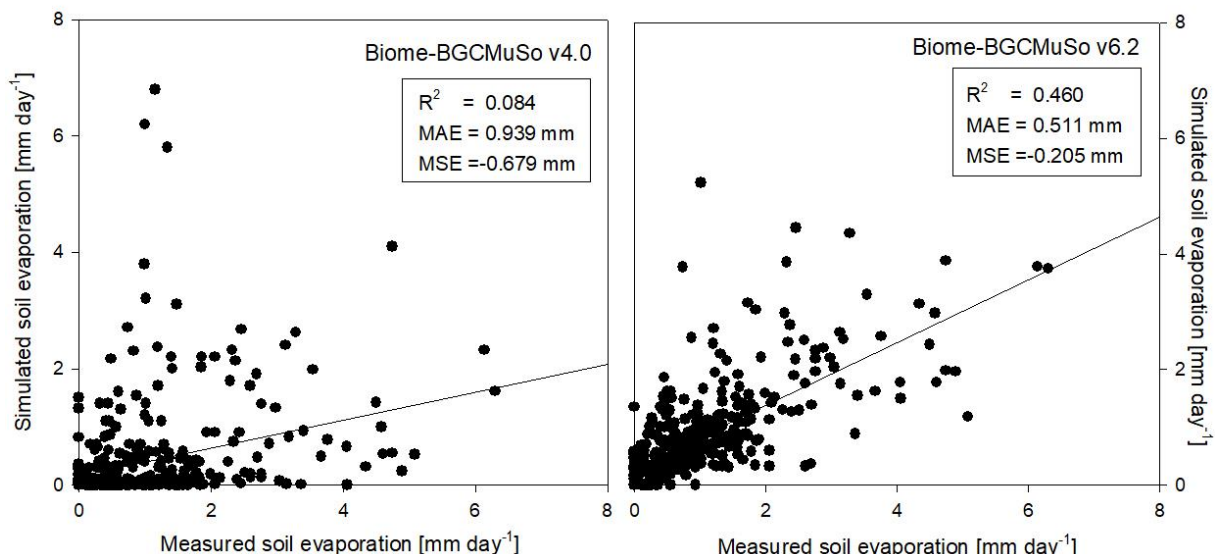


705
706 Figure 7: The simulated (blue line: v4.0; red line: v6.2) and the observed (grey dots) daily soil evaporation values at
707 Martonvásár during 2020. Vertical grey lines associated with the observations represent standard deviation of the
708 observations
709 observation from 6 lysimeter columns. The improved model clearly outperforms the earlier version.

710
711 In Figure 8 the simulated and the observed SWC at 10 cm depth are presented with the
712 daily sum of precipitation representing the bare soil simulation in Martonvásár, for 2020. The
713 soil water balance simulation seems to be realistic using v6.2, since the annual course
714 captures the low and high end of the observed values. In contrast, Biome-BGCMuSo v4.0
715 underestimates the range of SWC and provides overestimations during the growing season
716 (from spring to autumn). With a couple of exceptions, the simulated values using v6.2 fall
717 into the uncertainty range of the measured values defined by the standard deviation of the six
718 parallel measurements. This is not the case for the simulations with the 4.0 version.



719
720 | Figure 8: The simulated (blue line: v4.0; red line: v6.2) and the observed (grey dots) soil water content values at
721 | 10 cm depth (right y axis) with the daily sums of precipitation (left axis; black columns) during 2020 at Martonvásár
722 | lysimeter station. Vertical grey lines associated with the observations represent +/- one standard deviation around
723 | the observation. Simulated SWC using v6.2 is more consistent with the observations. The improved model clearly
724 | outperforms the earlier version in simulating soil water balance, than using v4.0.
725



726 |
727 | Figure 9: Comparison of the simulated (left: v4.0; right: v6.2) and observed daily soil evaporation (right) representing
728 | the means of measured data obtained from six weighing lysimeter columns with bare soil at Martonvásár in 2020. R^2 ,
729 | MAE and MSE denote the square of the linear correlation coefficient of determination, mean absolute error and
730 | mean signed error (bias) of the simulated values, respectively.
731 |
732 |

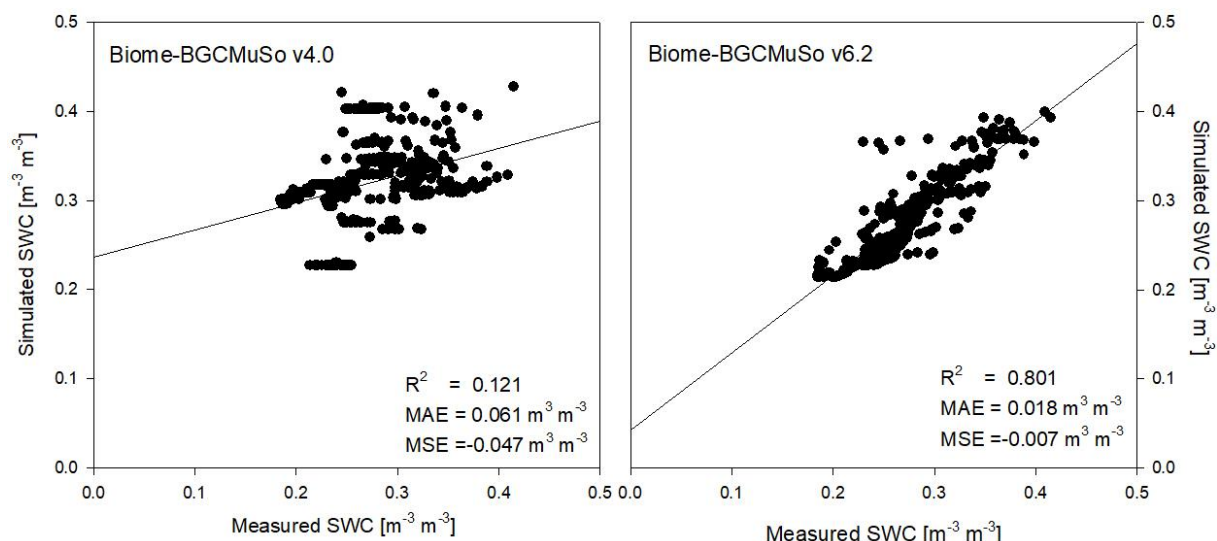
733 | Model performance was evaluated by quantitative measures such as square of linear
734 | correlation coefficient of determination (R^2), mean absolute error (MAE) and mean signed
735 | error (MSE). In Figure 9 the comparison of the simulated and the observed daily evaporation

736 is presented. Based on the performance indicators it is obvious that the simulation with new
737 model version (v6.2) is much closer to observations than the old version (v4.0). Biome-
738 BGCMuSo v6.2 slightly underestimated the observations.

739 In Figure 10 the comparison of the simulated and the observed daily SWC from the
740 lysimeter experiment is presented. Based on the model evaluation it seems that the simulation
741 with new model version is much closer to observation than with old version (4.0). The results
742 obtained from v4.02 are consistent with earlier findings about the incorrect representation of
743 the annual SWC cycle (Hidy et al., 2016; Sándor et al., 2017).

744 Throughout validation of the improved model based on observed SWC and ET
745 datasets from eddy covariance sites is planned to be published in an upcoming paper about the
746 plant related improvements under way.

747



749 Figure 10: Comparison of the simulated (left: v4.0; right: v6.2) and observed daily SWC representing the means of
750 measured data obtained from six weighing lysimeter columns with bare soil at Martonvásár in 2020. R^2 , MAE and
751 MSE denote the square of the linear correlation coefficient of determination, mean absolute error and mean signed
752 error (bias) of the simulated values, respectively.
753

754 **5.2 Evaluation of the soil nitrogen balance module and the simulated soil respiration**

755 Soil related developments were evaluated with a case study focusing on topsoil nitrate
756 content, soil N_2O efflux and soil respiration.

757 Experimental data were collected in a long-term fertilization experiment that was set
758 up in 1959 at Martonvásár, Hungary (N 47°18'41", E 18°46'50"). According to the FAO-
759 WRB classification system (IUSS Working Group, 2015), the soil is a Haplic Chernozem,
760 with 51.4% sand, 34% silt and 14.6% clay content. Bulk density is 1.47 g cm⁻³, pH(H₂O) is

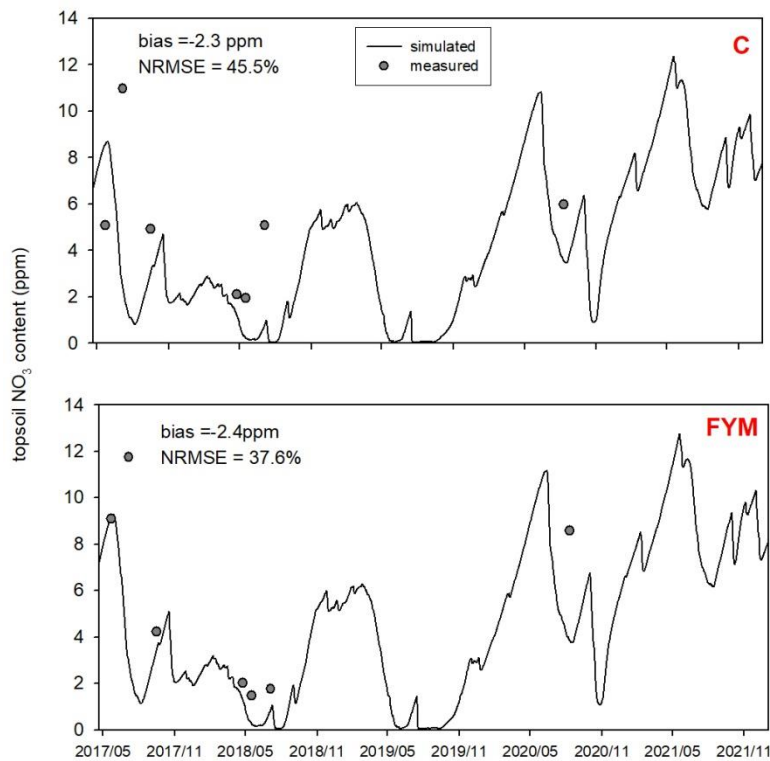
761 7.3. CaCO_3 content is 0–1%, and the mean soil organic matter content in the topsoil is 3.2%.
762 The plant-available macronutrient supply in the soil was poor for Phosphorus and medium to
763 good for Potassium, based on the ProPlanta plant nutrition advisory system (Fodor et al.,
764 2011). In the long-term fertilization experiment the treatments were arranged in a random
765 block design with 6×8 m plots in four replicates. Eight different treatments were set up:
766 control (zero artificial fertilizer applied), only N, only P and NPK – with farmyard manure;
767 absolute control (zero nutrient supply), only N, only P, NPK – without farmyard manure. The
768 crops in the four-year fertilizer cycles were maize in the 1st and 2nd years and winter wheat in
769 the 3rd and 4th years. Here we used data from the absolute control and from the farmyard
770 manure (FYM) treatments only. FYM was applied once every four years at a rate of 35 t ha^{-1}
771 in autumn.

772 Topsoil nitrate content was measured during 2017, 2018 and 2020 on a few occasions
773 by wet chemical reactions using a stream distillation method after KCl extraction of soil
774 samples (Hungarian Standards Institution MSZ 20135:1999; Akhtar et al., 2011).

775 Dynamic chamber based soil N_2O efflux observations were available from 2020 and
776 2021. The N_2O efflux measurements with a gas incubation time of 10 minutes were
777 performed by using a Picarro G2508 (Picarro, USA) cavity ring down spectrometer
778 (Christiansen et al. 2015; Zhen et al. 2021). The cylinder shaped transparent gas incubation
779 chamber was 16.5 cm in diameter and its height was 30 cm. N_2O flux measurements were
780 executed in 6 replicates per treatment on a biweekly (2020) and precipitation event-related
781 (2021) basis. Soil respiration was measured with the same Picarro gas analyser. Sampling
782 numbers and points were identical with those of the N_2O efflux measurements. CO_2 and N_2O
783 effluxes were calculated by linear equation (Widen and Lindroth, 2003) based on gas
784 concentration data.

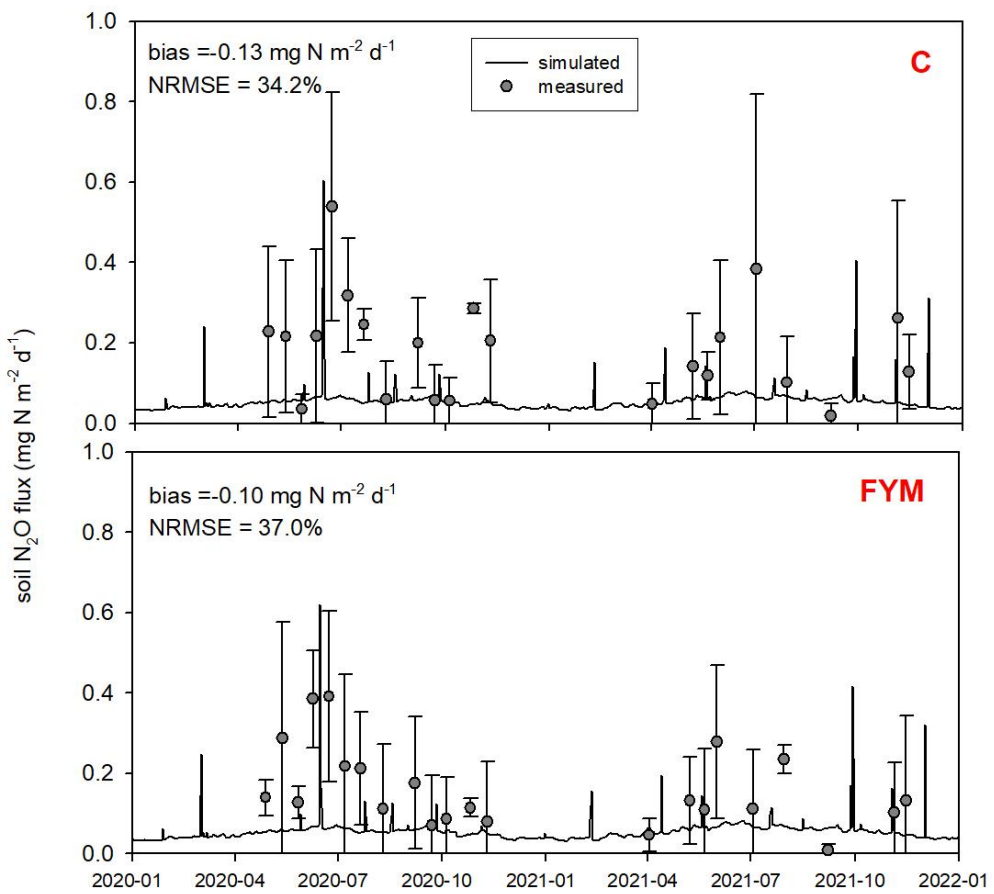
785 For the simulations we used maize parameterization from previous studies (Fodor et
786 al., 2021). Winter wheat parameterization was constructed based on a country-scale
787 optimization using the AgroMo software package (<https://github.com/hollarol/AgroMo>) and
788 the NUTS 3 level long-term (1991–2020) yield database of the Hungarian Central Statistical
789 Office. For nitrogen cycle related parameters we mainly used the values presented in the
790 User's Guide (Hidy et al., 2021). Two soil parameters were adjusted (coefficient of N_2O
791 emission for nitrification and $\text{N}_2/\text{N}_2\text{O}$ ratio multiplier for denitrification related N gas flux;
792 Del Grosso et al., 2000; Parton et al., 2001; Thomas et al., 2013; Hidy et al., 2021) to match
793 the simulated N_2O efflux to the observations.

794 Figure 11 shows the comparison of the simulated and observed NO_3 content of the
795 topsoil for the two selected treatments. The results indicate that the model underestimate the
796 topsoil NO_3 content both in the case of C and FYM (bias is -2.3 ppm and -2.4 ppm,
797 respectively) treatments, but the simulation error is in an acceptable range (NRMSE is 45.5%
798 and 37.6% for C and FYM, respectively).



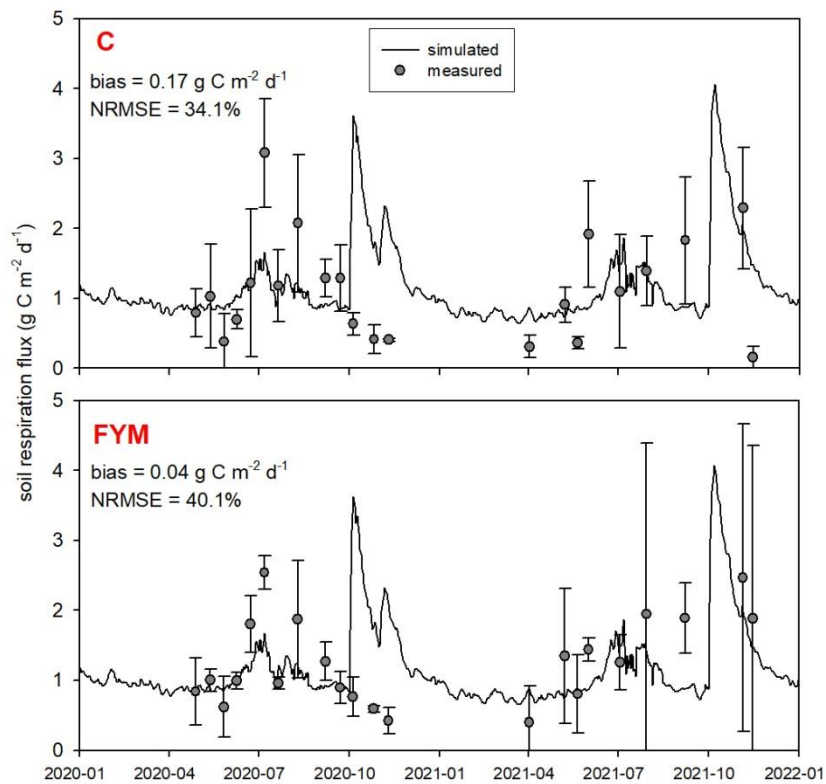
799
800 **Figure 11: Comparison of the simulated and observed NO_3 content of the topsoil for the absolute control (C; upper)**
801 **and for the farmyard manure (FYM; bottom) treatment between May 2017 and November 2021 at Martonvásár.**
802

803 Figure 12 shows the comparison of the observed and simulated N_2O efflux for the
804 2020-2021 time period. Measurement uncertainties are also indicated on the plot. Note that
805 the uncertainty of the observations (e.g. due to spatial heterogeneity and sample number, soil
806 disturbance, improper chamber design, methods of sample analysis) is remarkable due to
807 known features of the chamber technique (Chadwick et al. 2014; Pavelka et al. 2018). The
808 model captured more of the magnitude of N_2O efflux peaks and less of their timing. Overall
809 the model underestimated the observed values in both cases (bias is $-0.13 \text{ mg N m}^{-2} \text{ day}^{-1}$ and
810 $-0.1 \text{ mg N m}^{-2} \text{ day}^{-1}$ for C and FYM, respectively), with NRMSE of 32.4% and 37.6% for C
811 and FYM, respectively.



812
 813 **Figure 12: Comparison of the simulated and observed soil N_2O efflux for two treatments: absolute control (C; upper)**
 814 **and application of farmyard manure (FYM; bottom) between January 2020 and December 2021 at Martonvásár.**
 815 **Whiskers indicate the uncertainty (\pm one standard deviation) of the measurements.**

816
 817 **Figure 13 presents the comparison of the observed and simulated soil respiration for**
 818 **the same time period as for the soil N_2O efflux. Observation uncertainty is indicated that**
 819 **represents one standard deviation of the replicates. The model mostly captured the magnitude**
 820 **and variability of soil respiration flux. The model overestimated the observed values in both**
 821 **cases with bias of $0.17 \text{ g C m}^{-2} \text{ day}^{-1}$ and $0.04 \text{ g C m}^{-2} \text{ day}^{-1}$ for C and FYM, respectively. The**
 822 **NRMSE is 34.1% and 40.1% for C and FYM, respectively. It is interesting to note that the**
 823 **observations and the simulations are particularly different after harvest time in both years (i.e.**
 824 **beginning of October). The simulated respiration have peaks are corresponding to harvest**
 825 **when the amount of litter sharply increases due to the byproducts left behind (decomposition**
 826 **of residues left on the site after harvest are accounted for in the model). The chamber based**
 827 **CO_2 efflux data did not really show similar peaks likely because of methodological issues**
 828 **(litter is removed from the soil surface before placing of the chambers).**



829

830 **Figure 13: Comparison of the simulated and observed soil respiration flux for two treatments: absolute control (C;**
 831 **application of farmyard manure (FYM; bottom) between January 2020 and December 2021 at**
 832 **Martonvásár. Whiskers indicate the uncertainty (\pm one standard deviation) of the measurements.**

833

834 Overall, the model provided nitrate content, N_2O emission and soil respiration
 835 simulation results that are consistent with the observations. The model was capable of
 836 estimating the observed values with a comparable efficiency reported in similar studies
 837 (Gabrielle et al., 2002; Andrews et al., 2020).

838 **5.3**

839 **5.2 Sensitivity analysis and optimization of the soil biogeochemistry scheme**

840

841 —————— Here we present another case study that provides insight into the functioning of the
 842 converging cascade (decomposition) scheme that is implemented in Biome-BGCMuSo v6.2.
 843 A large scale in silico experiment is also presented where the main aim was to perform model
 844 self-initialization (i.e. spinup) at the country scale (for the entire area of Hungary) where the
 845 resulting soil organic matter pools are expected to be consistent with the observations.

846

847 The observation based, gridded, multi-layer SOC database of Hungary (DOSoReMI

database; Pásztor et al., 2020; see Supplementary material Figures S3-S42020) as well as the

848 FORESEE meteorological database (Kern et al., 2016) was used for the sensitivity analysis of
849 the soil scheme as well as for optimizing the most important soil parameters when the model
850 was calibrated referring to the observation based SOC values simulation. As a first step, the
851 area of the country was divided into 1104 grid cells (regular grid with 0.1° by 0.1° resolution,
852 corresponding to an approximately 10 km resolution). The 1104 grid cells of the DOSoReMI
853 database were grouped based on their dominant land-use type (cropland, grassland, forest
854 based on CORINE-2018²⁰¹² database; EEA, 2021; Supplementary material Figures S1-S2)
855 as well as the soil texture class (12 classes according to the USDA system; USDA, 1987) and
856 SOC content (high and low; high is greater than the group mean while low is less than the
857 mean) of the topsoil (0-30 cm layer). As some of the theoretically possible 72 groups had no
858 members (e.g. there is no soil in Hungary with sandy-clay texture) soils of the 1104 grid cells
859 were categorized into 51 groups. For each group one single cell (so-called representative cell)
860 was selected based on the topsoil SOC content. The representative cell was the one with the
861 smallest absolute deviation from the group mean SOC content. (Land use maps for Hungary
862 are presented in the Supplementary Material Section 10: Figure S1-S2).

863 Grassland ecophysiological parameterization without management was used in the
864 spinup phase to initialize SOC pools for croplands. For for the transient spinup phase cropland
865 parameterization was used, and with fertilization, harvest and ploughing, planting and harvest
866 settings in the transient phase. In case of grasslands, both during the spinup and transient
867 phases grassland parameterization was used, and in the transient phase mowing was assumed
868 (once a year. In in case of forests generic deciduous broadleaf forest parameterization was
869 used for both spinup and transient phases with thinning, and in the latter transient phase. For
870 our parameterization presented in the MS the thinning was set. Parameterization was
871 performed based on generic, plant functional type specific ecophysiological parameter sets
872 published by parameters that were created based on the original parameterization of White et
873 al. (2000) served as starting points. These. Biome-BGCMuSo specific parameter sets are
874 available at the website of the model¹.

875 Soil parameters in Biome-BGCMuSo v66.2 were classified into six groups: (1) 4
876 generic soil parameters, (2) 24 decomposition-nitrification-denitrification related parameters,
877 (3) 14 rate scalars for the converging (decomposition) cascade scheme, (4) 19 soil moisture
878 related parameters, (5) 7 methane related parameters and (6) 11 soil composition and

¹ http://nimbus.elte.hu/bbgc/files/generic_EPC_set_6.24.zip

879 characteristic values (can be set layer by layer). Detailed description and proposed value of
880 each soil parameters can be found in the User's Guide (Hidy et al., 2021).

881

882

883
884
885
886
887

Table 1: Soil parameters of Biome-BGCMuSo v6.2 (referring to SOC simulation) that were used during the sensitivity analysis. The **VALUE column shows the originally proposed values (Hidy et al., 2021). See Figure 4 for explanation on the compartment names. The parameters that were included in the 2nd phase of the sensitivity analysis are marked with bold letters (see text).**

GROUP	PARAMETER NAME	ABBREVIATION	VALUE
Generic soil parameters	C:N ratio of stable soil pool (soil4)	soil4CN	12
	NH4 mobile proportion	amMP	0.1
	aerodynamic resistance	potRair	107
Decomposition, nitrification, denitrification parameters	parameter 1 for temperature response function of decomp.	Tp1decomp	1.75
	parameter 2 for temperature response function of decomp.	Tp2decomp	17
	parameter 3 for temperature response function of decomp.	Tp3decomp	2.6
	parameter 4 for temperature response function of decomp.	Tp4decomp	40
	minimum T for decomposition and nitrification	Tp5decomp	-5
	e-folding depth of decomposition rate's depth scalar	EFD	10
	net mineralization proportion of nitrification	NITRnetMINER	0.2
	maximum nitrification rate	NITRmaxRATE	0.1
	coefficient of N2O emission of nitrification	NITRratioN2O	0.02
	parameter 1 for pH response function of nitrification	pHp1nitrif	0.15
	parameter 2 for pH response function of nitrification	pHp2nitrif	1
	parameter 3 for pH response function of nitrification	pHp3nitrif	5.2
	parameter 4 for pH response function of nitrification	pHp4nitrif	0.55
	parameter 1 for Tsoil response function of nitrification	Tp1nitrif	1
	parameter 2 for Tsoil response function of nitrification	Tp2nitrif	12
	parameter 3 for Tsoil response function of nitrification	Tp3nitrif	2.6
	parameter 4 for Tsoil response function of nitrification	Tp4nitrif	2.6
	minimum WFPS for scalar of nitrification calculation	minWFPS	0.1
Rate scalars	lower optimum WFPS for scalar of nitrification	opt1WFPS	0.45
	higher optimum WFPS for scalar of nitrification	opt2WFPS	0.55
	minimum value for saturated WFPS scalar of nitrification	minWFPSscalar	0.2
	soil respiration related denitrification rate	DENITcoeff	0.05
	denitrification related N2/N2O ratio multiplier	DNratioN2O	2
	critical WFPS value for denitrification	critWFPSdenitr	0.50
	respiration fractions for fluxes between compartments (I1s1)	RFI1s1	0.39
	respiration fractions for fluxes between compartments (I2s2)	RFI2s2	0.55
	respiration fractions for fluxes between compartments (I4s3)	RFI4s3	0.29
	respiration fractions for fluxes between compartments (s1s2)	RFs1s2	0.28
	respiration fractions for fluxes between compartments (s2s3)	RFs2s3	0.46
	respiration fractions for fluxes between compartments (s3s4)	RFs3s4	0.55
	potential rate constant of labile litter pool	RCS1	0.7
	potential rate constant of cellulose litter pool	RCS2	0.07
	potential rate constant of lignin litter pool	RCS3	0.014
	potential rate constant of fast microbial recycling pool	RCS4	0.07
	potential rate constant of medium microbial recycling pool	RCS5	0.014
	potential rate constant of slow microbial recycling pool	RCS6	0.0014
	potential rate constant of recalcitrant SOM (humus) pool	RCS7	0.0001
	potential rate constant of physical fragmentation of wood	RCS8	0.001
	maximum height of pond water	MP	5
	curvature of soil stress function	q	1
	fraction of dissolved part of S1 organic matter	fD1	0.005
	fraction of dissolved part of S2 organic matter	fD2	0.004
	fraction of dissolved part of S3 organic matter	fD3	0.003
	fraction of dissolved part of S4 organic matter	fD4	0.002
	mulch parameter: critical amount	CAmulch	1
	parameter 1 for mulch function	p1mulch	100
	parameter 2 for mulch function	p2mulch	0.75
	parameter 3 for mulch function	p3mulch	0.75
	mulch parameter: evaporation reduction	ERmulch	0.5

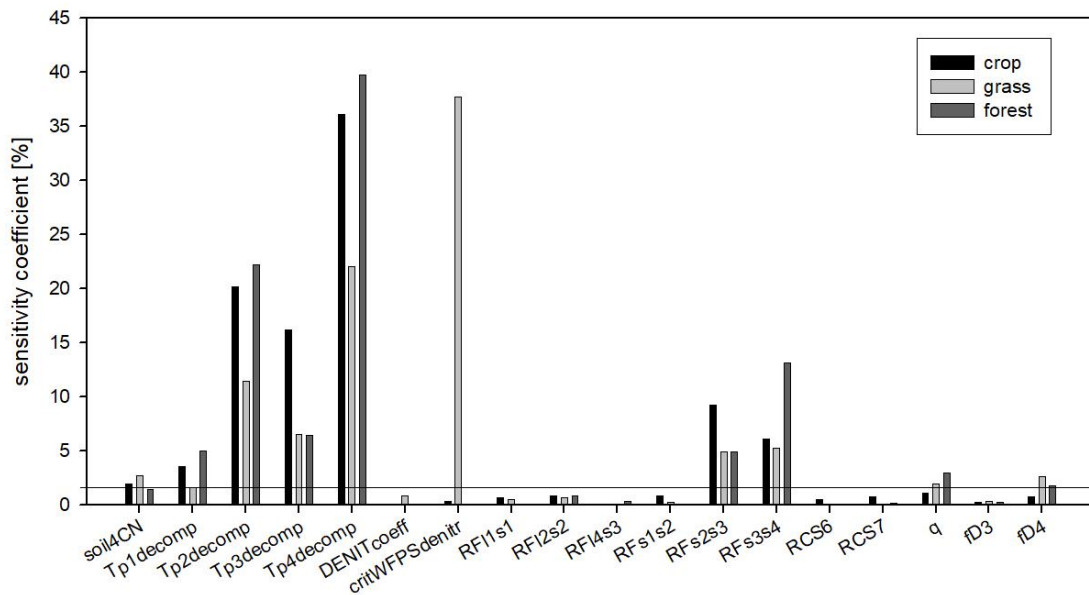
888 As methane simulation was not the subject of the present case study we neglected the
889 related parameters. Regarding to the soil composition and characteristic values we used the
890 DOSoReMI database (Pásztor et al., 2020). From the remaining 61 parameters soil depth,
891 runoff curve number, the three soil moisture related parameters (tipping bucket method) were
892 not included ~~in the~~ analysis. ~~The groundwater module was switched off-Groundwater~~
893 ~~parameters were inactive~~ in this case (no groundwater is assumed) ~~and the related~~
894 ~~which means that those~~ parameters were not studied. The remaining 53 parameters ~~were~~ used in
895 ~~the~~ sensitivity analysis and are listed in Table 1.

896 As a first step sensitivity analysis was carried out for the selected 53 soil parameters
897 by running the Biome-BGCMuSo v6.2 model in spinup mode until a quasi-equilibrium in the
898 total SOC is reached (that is the usual logic of the spinup run). The model was run for each
899 representative cell 2000 times with varying model parameters using Monte-Carlo method.
900 Each model parameters were varied randomly within the $\pm 10\%$ range of their initial values
901 that were inherited from the Biome-BGC model or were set according to the literature. The
902 least square linearization (LSL) method (Verbeeck et al., 2006) was used for dividing output
903 uncertainty into its input parameter related variability. As result of the LSL method, the total
904 variance of the model output and the sensitivity coefficient of each parameter can be
905 determined. Sensitivity coefficients show the percent of total variance for which the given
906 parameter is responsible.

907 In order to simplify the workflow and decrease the degree of freedom another
908 sensitivity analysis was performed. In this second step, the sensitive parameters (sensitivity
909 coefficient $> 1\%$ for at least one land use type; a total of 18 parameters) were used in the
910 following sensitivity analysis with 6000 iteration steps. These 18 parameters are marked with
911 bold letters in Table 1.

912 Figure [1410](#) shows the summary of the second sensitivity analysis where the overall
913 importance of the parameters ~~is~~ calculated as the mean of all selected pixels in a given land
914 use category. It can be seen in Figure [410](#) that from the 18 parameters (selected during the
915 first phase) soil carbon ratio of the recalcitrant pool (soil4CN), the temperature dependence
916 parameters of decomposition function (Tp1decomp, Tp2decomp, Tp3decomp, Tp4_decomp)
917 and the respiration fraction of S2-S3 and S3-S4 decomposition process (RFs2s3 and RFs3s4),
918 the curvature of soil stress function ($q_{soilstress}$) and the fraction of dissolved part of S4 organic
919 matter (fD4) are the most important for all land use types. Among the other parameters the
920 critical WFPS of denitrification (critWFPSdentir) for grasslands has a remarkably high
921 sensitivity (greater ~~than~~
~~that~~ 35%). It means that in case of grasslands the nitrogen availability

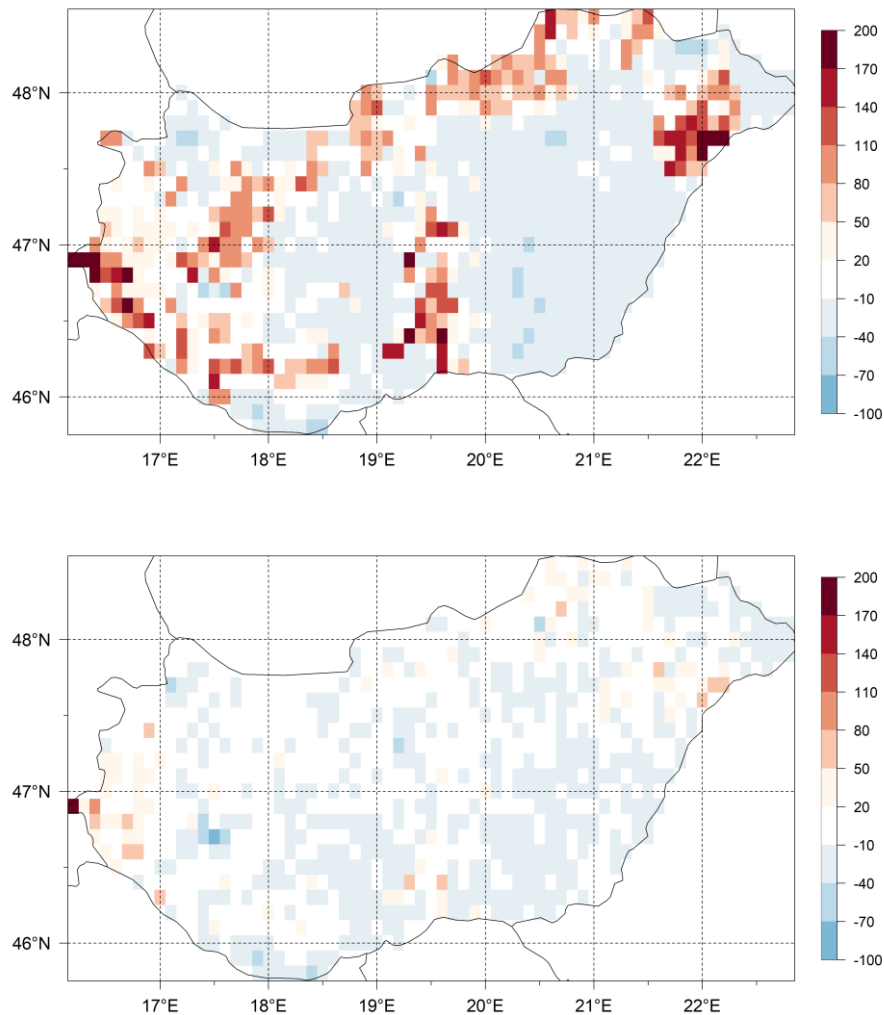
922 seems to be an important limitation of the primary production, probably because there are
 923 only natural sources of nitrogen (no fertilization is assumed here), and the rooting zone is
 924 shallower than in case of forest which involves limited mineralized N access. Thus, in case of
 925 higher values of critical WFPS of denitrification, the simulated production of the grassland
 926 (and therefore the final SOC) seems to be significantly underestimated.



927
 928 | **Figure 1410:** The sensitivity coefficients of the soil parameters as the result of the sensitivity analysis. Black columns
 929 refer to the crop, light grey to the grass and dark grey to the forest simulations. The sensitivity coefficients are
 930 calculated as the mean pixel level sensitivity coefficient for the given land use type. Horizontal line indicates the 5%
 931 threshold that was used to select the final parameter set **for that is subject to** optimization.

932
 933 The selected ten, soil biogeochemistry related parameters were optimized for each of
 934 the 51 groups separately, using maximum likelihood estimation. For each group, the
 935 parameter set providing the smallest deviation between the simulated and the observed values
 936 of the weighted average SOC content (weight factor of 5 is used for the 0-30 cm, and weight
 937 factor of 1 is used for the 30-60 cm soil layers) was considered to be the final (optimized)
 938 model parameter set.

939 The differences of the simulated and observed SOC content for the 0-30 cm layer
 940 (SOC0-30) using the initial (Table 1) and final soil parameters (not shown here) are presented
 941 in Figure 1511. On the upper plot the signed relative error of SOC0-30 simulation before
 942 optimization, while on the lower figure the signed relative error of SOC0-30 simulation after
 943 optimization can be seen. It is clearly visible that because of optimization the overestimation
 944 of the SOC0-30 simulation significantly decreased.



945
946
947
948
949

Figure 154: Differences (expressed as signed relative error, %) between the simulated and observed SOC data for the 0-30 layer (SOC0-30) using the initial (upper map) and optimized (lower map) soil parameters. The maps present the signed relative error in percent. Visual comparison of the maps reveals the success of the optimization in terms of capturing the overall SOC for the whole country area.

950

951 We do not claim of course that the optimized parameters have universal value. Site
952 history is neglected during the spin up simulations, and we use many simplifications like
953 disregarding non-existent land use change, present-day ecophysiological parameterization etc.
954 In this sense, the optimized parameter set can be best considered as a pragmatic solution to
955 provide initial conditions (equilibrium SOC pools) for the model at the country scale that is
956 consistent with the observations.

957 **6. Concluding remarks**

958 In this paper, we presented a detailed description of the soil hydrology and
 959 carbon/nitrogen budget related developments of the Biome-BGCMuSo v6.2 terrestrial
 960 ecosystem model. We mostly focused on changes relative to the previously published Biome-
 961 BGCMuSo v4.0 (Hidy et al., 2016), but our intention was also to provide a complete,
 962 standalone reference for the modelling community with mathematical equations (detailed in
 963 the Supplementary Material). Table 2 summarizes the structural changes that we made during
 964 the developments starting from Biome-BGC v4.1.1 also including the previously published
 965 Biome-BGCMuSo v4.0 (Hidy et al., 2016).

966

967 | **Table 2. Comparison of the internal processes simulated in model structural solutions for Biome-BGC 4.1.1, Biome-
 968 BGCMuSo v4.0 and in Biome-BGCMuSo v6.2.**

Routine	original Biome-BGC	Biome-BGCMuSo v4.0	Biome-BGCMuSo v6.2
Runoff	no	based on simple, empirical formulation	distinguishing Hortonian and Dunne runoff
Pond water	no	simple solution	development of pond water formation (based on infiltration capacity)
Soil evaporation	Based on Penman-Monteith equation Calculation of the actual evaporation from the potential evaporation and the square root of time elapsed since the last precipitation.	Based on Penman-Monteith equation Calculation of the actual evaporation from the potential evaporation and the square root of time elapsed since the last precipitation.	Based on Penman-Monteith equation Parameterization possibility of actual aerodynamic resistance. Introduction of an upper limit for daily potential evaporation that is determined by the available energy. Calculation of the actual evaporation is based on the method RitchieRitehe (1981). Simulation of the reducing effect of surface residue or mulch cover on bare soil evaporation
Transpiration	Transpiration from one-layer bucket soil	Transpiration from 7-layers soil based on soil stress	Transpiration from 10-layers soil based on available water
Groundwater	no	Simple groundwater simulation.	Improvement of the simulation of groundwater effect (using capillary fringe). Introduction of two different methods.
Soil moisture stress	no	Relative SWC data is used to calculate soil water stress. The hygroscopic water, the wilting point, the field capacity and the saturation values of the soil layers can be defined in the input file layer by layer. The soil moisture stress index is affected by the length and the day since the drought event lasted.	The hygroscopic water, the wilting point, the field capacity and the saturation values of the soil layers can be defined in the input file layer by layer. The soil moisture stress index is affected by the length and the severity of the drought event, aggravated by the extreme temperature. Introduction of the soil curvature parameters to provide mechanism for soil texture dependent drought stress since it can affect the shape of the soil stress function.

			Normalized SWC data are used to calculate soil moisture stress index.
Organic carbon and nitrogen	One layer soil module with one organic carbon and nitrogen pool.	Multi-layered soil module without soil carbon and nitrogen profile.	Instead of defining a single litter, soil organic carbon and nitrogen pool, separate carbon and nitrogen pools for each soil layer in the form of soil organic matter and litter were implemented. Separation of above- and belowground litter pools. Litter and soil decomposition fluxes (carbon and nitrogen fluxes from litter to soil pools) are calculated layer by layer, depending on the actual temperature and SWC of the corresponding layers. Leaching of dissolved organic carbon and nitrogen.
Inorganic nitrogen	One layer soil module with one mineralized N pool.	Multi-layer soil module with an empirical inorganic N-profile (no layer-by-layer calculations, only estimation of the subpools in the different soil layer based on the rootlength proportion).	Separation of ammonium (NH_4) and nitrate (NO_3) soil pools instead of a general mineralized nitrogen pool. Nitrification fluxes are calculated layer by layer, depending on the actual pH, temperature and SWC of the given layers. Denitrification fluxes are calculated layer by layer, depending on the depth, actual temperature and SWC of the given layers.

969

970

971 Earlier model versions used a soil hydrology scheme based on the Richards equation,
 972 but the results were not satisfactory. Sándor et al. (2017) presented results from the first major
 973 grassland model intercomparison project (executed within the frame of FACCE MACSUR)
 974 where Biome-BGCMuSo [v22.2](#) was used. That study demonstrated the problems associated
 975 with proper representation of soil water content that was a common shortcoming of all
 976 included models. In the Hidy et al. (2016) paper, where the focus was on Biome-BGCMuSo
 977 v4.0, the SWC related figures clearly indicated problems with the simulations compared to
 978 observations. The SWC amplitude was not captured well which clearly influences drought
 979 stress, decomposition, and other SWC driven processes like nitrification and denitrification.
 980 For the latter two processes this is especially critical as they are associated with contrasting
 981 SWC regimes (nitrification is an aerobic, while denitrification is an anaerobic process). This
 982 is a good example for erroneous internal process representation that may lead to improper
 983 results. Note that the currently used functions for nitrification/denitrification are also subject
 984 to uncertainty that needs to be addressed in the future (Heinen, 2006). Nevertheless, the

985 presented model developments might contribute to a more realistic soil process simulations
986 and improved results.

987 Algorithm ensemble approach is already implemented in Biome-BGCMuSo.
988 Algorithm ensemble means that the user has more than one option for the representation of
989 some processes. Biome-BGCMuSo v6.2 has alternative phenology routines (Hidy et al.,
990 2012), two alternative methods for soil temperature (Hidy et al., 2016), soil hydrology
991 (described in this study), photosynthesis and soil moisture stress calculation. We plan to
992 extend the algorithm ensemble by providing alternative decomposition schemes to the model.
993 One possibility is the implementation of a CENTURY-like structure (Koven et al., 2013) that
994 is a promising direction and might improve the quality of the equilibrium (spin-up)
995 simulations and the simulated N mineralization related to SOM decomposition. Reported
996 problems related to the rapid decomposition of litter in the current model structure (Bonan et
997 al., 2013) needs to be addressed in future model versions as well.

998 Plant growth and allocation related developments were not addressed in this study but
999 of course has many inferences with the presented model logic (i.e. parameterization and
1000 related primary production defines the amount and quality of litter, etc.). A forthcoming
1001 publication will provide a comprehensive overview on the plant growth and senescence
1002 related model modifications where elements from crop models are also included.

1003 Biome-BGCMuSo is still an open source model that can be freely downloaded from
1004 its website with a detailed User's Guide and other supplementary files. We also encourage
1005 users to test the so-called RBBGCMuso package (available at GitHub) that has many
1006 advanced features to support model application and optimization. A graphical environment,
1007 called AgroMo (also available at GitHub: <https://github.com/hollarol/AgroMo>) was also
1008 developed around Biome-BGCMuSo to help users in carrying out simulations either with site
1009 specific plot scale data or with gridded databases representing large regions.

1010
1011

1012 **Code and data availability**

1013 The current version of Biome-BGCMuSo, together with sample input files and detailed User's
1014 Guide are available from the website of the model: <http://nimbus.elte.hu/bbgc/download.html>
1015 under the GPL-2 licence. Biome-BGCMuSo v6 is also available at GitHub:
1016 https://github.com/bpbond/Biome-BGC/tree/Biome-BGCMuSo_v6. The exact version of the
1017 model (v6.2 alpha) used to produce the results used in this paper is archived on Zenodo

1018 (https://doi.org/10.5281/zenodo.5761202). Experimental data and model parameterization
1019 used in the study are available from the corresponding author upon request.

1020

1021

1022 **Authors' Contributions**

1023 Hidy developed Biome-BGCMuSo, maintained the source code and executed the sample
1024 simulations. The study was conceived and designed by Hidy, Barcza and Fodor, with
1025 assistance from Ács, Dobor and Hollós. It was directed by Hidy and Barcza-. Ács and Dobor
1026 contributed with model benchmarking. Hollós participated with the construction of a
1027 modeling framework for Biome-BGCMuSo. -Filep, Incze, Zacháry and Pásztor contributed
1028 with experimental data. Hidy, Barcza, Fodor and Merganičová prepared the manuscript and
1029 the supplement with contributions from all co-authors. All authors reviewed and approved the
1030 present article and the supplement.

1031

1032

1033 **Acknowledgements**

1034 The research was funded by the Széchenyi 2020 programme, the European Regional
1035 Development Fund and the Hungarian Government (GINOP-2.3.2-15-2016-00028). This
1036 research was supported by the NFDI Fund FK 20 Grant Project no. 134547 as well. Also
1037 supported by grant "Advanced research supporting the forestry and wood-processing sector's
1038 adaptation to global change and the 4th industrial revolution", No.
1039 CZ.02.1.01/0.0/0.0/16_019/0000803 financed by OP RDE". KM was also financed by the
1040 project: "Scientific support of climate change adaptation in agriculture and mitigation of soil
1041 degradation" (ITMS2014+ 313011W580) supported by the Integrated Infrastructure
1042 Operational Programme funded by the ERDF. We are grateful to Galina Churkina for
1043 reviewing this manuscript.

1044

1045

1046 **References**

1047 [Akhtar, M.H., Firyal O. Qureshi, T., Ashraf, M. Y., Akhter, J., Haq, A.: Rapid and
1048 Inexpensive Steam Distillation Method for Routine Analysis of Inorganic Nitrogen in
1049 Alkaline Calcareous Soils, Communications in Soil Science and Plant Analysis 42, 920-931,
1050 \[https://doi.org/10.1080/00103624.2011.558961, 2011\]\(https://doi.org/10.1080/00103624.2011.558961\)](https://doi.org/10.1080/00103624.2011.558961)

1051 [Andrews, J.S. , Sanders, Z.P. , Cabrera, M.L., Hill, N.S., Radcliffe, D.E.: Simulated nitrate
1052 leaching in annually cover cropped and perennial living mulch corn production systems,
1053 Journal of Soil and Water Conservation, 75 \(1\), 91-102, \[https://doi.org/10.2489/jswc.75.1.91,
1054 2020.\]\(https://doi.org/10.2489/jswc.75.1.91\)](https://doi.org/10.2489/jswc.75.1.91)

1055 [Asseng, S., Ewert, F., Rosenzweig, C., Jones, J.W., Hatfield, J.L., Ruane, A.C., Boote, K.J.,
1056 Thorburn, P.J., Rötter, R.P., Cammarano, D., Brisson, N., Basso, B., Martre, P., Aggarwal,
1057 P.K., Angulo, C., Bertuzzi, P., Biernath, C., Challinor, A.J., Doltra, J., Gayler, S., Goldberg,
1058 R., Grant, R., Heng, L., Hooker, J., Hunt, L.A., Ingwersen, J., Izaurralde, R.C., Kersebaum,
1059 K.C., Müller, C., Naresh Kumar, S., Nendel, C., O'Leary, G., Olesen, J.E., Osborne, T.M.,
1060 Palosuo, T., Priesack, E., Riponche, D., Semenov, M.A., Shcherbak, I., Steduto, P., Stöckle, C.,
1061 Stratonovitch, P., Streck, T., Supit, I., Tao, F., Travasso, M., Waha, K., Wallach, D., White,
1062 J.W., Williams, J.R., Wolf, J.: 2013. Uncertainty in simulating wheat yields under climate
1063 change., Nature Climate Change 3, 827–832, \[https://doi.org/10.1038/nclimate1916, 2013.\]\(https://doi.org/10.1038/nclimate1916\)
1064 <https://doi.org/10.1038/nclimate1916>](https://doi.org/10.1038/nclimate1916)

1065 <https://doi.org/10.1038/nclimate1916>

1066 <https://doi.org/10.1038/nclimate1916>

1067 <https://doi.org/10.1038/nclimate1916>

1068 <https://doi.org/10.1038/nclimate1916>

1069 <https://doi.org/10.1038/nclimate1916>

1070 <https://doi.org/10.1038/nclimate1916>

1071 <https://doi.org/10.1038/nclimate1916>

1072 <https://doi.org/10.1038/nclimate1916>

1073 <https://doi.org/10.1038/nclimate1916>

1074 <https://doi.org/10.1038/nclimate1916>

1075 <https://doi.org/10.1038/nclimate1916>

1076 <https://doi.org/10.1038/nclimate1916>

1077 <https://doi.org/10.1038/nclimate1916>

1078 <https://doi.org/10.1038/nclimate1916>

1079 <https://doi.org/10.1038/nclimate1916>

1080 <https://doi.org/10.1038/nclimate1916>

1081 <https://doi.org/10.1038/nclimate1916>

1082 <https://doi.org/10.1038/nclimate1916>

1083 <https://doi.org/10.1038/nclimate1916>

1084 <https://doi.org/10.1038/nclimate1916>

1085 <https://doi.org/10.1038/nclimate1916>

1086 <https://doi.org/10.1038/nclimate1916>

1087 <https://doi.org/10.1038/nclimate1916>

1088 <https://doi.org/10.1038/nclimate1916>

1089 <https://doi.org/10.1038/nclimate1916>

1090 <https://doi.org/10.1038/nclimate1916>

1091 <https://doi.org/10.1038/nclimate1916>

1092 <https://doi.org/10.1038/nclimate1916>

1093 <https://doi.org/10.1038/nclimate1916>

1094 <https://doi.org/10.1038/nclimate1916>

1095 Christiansen, J.R., Outhwaite, J., Smukler, S.M.: Comparison of CO₂, CH₄ and N₂O soil-
1096 atmosphere exchange measured in static chambers with cavity ring-down spectroscopy and
1097 gas chromatography, *Agriculture Forest Meteorology*, 211–212, 48–57,
1098 <https://doi.org/10.1016/j.agrformet.2015.06.004>, 2015.

1099 Dietze, M.: 2013. Gaps in knowledge and data driving uncertainty in models of
1100 photosynthesis. *Photosynthesis Research* 119, 3–14. <https://doi.org/10.1007/s11120-013-9836-z>

1103 Dolezal, F., Hernandez-Gomis, R., Matula, S., Gulamov, M., Miháliková, M., Khodjaev, S.: 2018.
1104 Actual Evapotranspiration of Unirrigated Grass in a Smart Field Lysimeter. *Vadose Zone Journal* 17, 1–13. <https://doi.org/10.2136/vzj2017.09.0173>, 2018.
1105 <https://doi.org/10.2136/vzj2017.09.0173>

1108 EEA, 2021. "CoORDinated" Co ORdinated INformation on the Environment (CORINE) Land
1109 Cover 2012, Version 18.4. European Commission - Directorate-General for Internal Market,
1110 Industry, Entrepreneurship and SMEs (DG-GROW, data owner)." European Environment
1111 Agency (EEA, data custodian). [URL: http://land.copernicus.eu/pan-european/corine-land-cover/clc-2012](http://land.copernicus.eu/pan-european/corine-land-cover/clc-2012). Accessed 17 February 2021. [URL: http://land.copernicus.eu/pan-european/corine-land-cover/clc-2012](http://land.copernicus.eu/pan-european/corine-land-cover/clc-2012). Accessed 17 February 2021.

1115 Ewert, F., Rötter, R.P., Bindi, M., Webber, H., Trnka, M., Kersebaum, K.C., Olesen, J.E., van
1116 Ittersum, M.K., Janssen, S., Rivington, M., Semenov, M.A., Wallach, D., Porter, J.R.,
1117 Stewart, D., Verhagen, J., Gaiser, T., Palosuo, T., Tao, F., Nendel, C., Roggero, P.P.,
1118 Bartošová, L., Asseng, S.: 2015. Crop modelling for integrated assessment of risk to food
1119 production from climate change. *Environmental Modelling & Software*, 72, 287–303.
1120 <https://doi.org/10.1016/j.envsoft.2014.12.003>, 2015.
1121 <https://doi.org/10.1016/j.envsoft.2014.12.003>

1123 Farquhar, G.D., von Caemmerer, S., Berry, J.A.: 1980. A biochemical model of
1124 photosynthetic CO₂ assimilation in leaves of C3 species. *Planta*, 149, 78–90.
1125 <https://doi.org/10.1007/BF00386231>, 1980. <https://doi.org/10.1007/BF00386231>

1127 Franke, J., Müller, C., Elliott, J., Ruane, A., Jägermeyr, J., Balkovič, J., Ciais, P., Dury, M.,
1128 Falloon, P., Folberth, C., François, L., Hank, T., Hoffmann, M., Izaurrealde, R., Jacquemin, I.,
1129 Jones, C., Khabarov, N., Koch, M., Moyer, E.: 2020. The GGCMI Phase 2 experiment:
1130 Global gridded crop model simulations under uniform changes in CO₂, temperature, water,
1131 and nitrogen levels (protocol version 1.0). *Geoscientific Model Development* 13, 2315–
1132 2336, <https://doi.org/10.5194/gmd-13-2315-2020>, 2020. <https://doi.org/10.5194/gmd-13-2315-2020>

1135 Fodor, N., Csathó, P., Árendás, T., Németh, T.: New environment-friendly and cost-saving
1136 fertiliser recommendation system for supporting sustainable agriculture in Hungary and
1137 beyond, *Journal of Central European Agriculture*, 12, 53–69, 2011.

1138 Fodor, N., Pásztor, L., Szabó, B., Laborczi, A., Pokovai, K., Hidy, D., Hollós, R., Kristóf, E.,
1139 Kis, A., Dóbor, L., Kern, A., Grünwald, T., Barcza, Z.: 2021. Input database related
1140 uncertainty of Biome-BGCMuSo agro-environmental model outputs. *International Journal of
1141 Digital Earth*, 14, 1582–1601, <https://doi.org/10.1080/17538947.2021.1953161>, 2021–20.
1142 <https://doi.org/10.1080/17538947.2021.1953161>

1145
1146 Friedlingstein, P., Joel, G., Field, C.B., Fung, I.Y.: 1999. Toward an allocation scheme for
1147 global terrestrial carbon models. *Global Change Biology* 5, 755–770,
1148 <https://doi.org/10.1046/j.1365-2486.1999.00269.x>, 1999. <https://doi.org/10.1046/j.1365-2486.1999.00269.x>

1150
1151 Friedlingstein, P., O'Sullivan, M., Jones, M. W., Andrew, R. M., Hauck, J., Olsen, A., Peters,
1152 G. P., Peters, W., Pongratz, J., Sitch, S., Le Quéré, C., Canadell, J. G., Ciais, P., Jackson, R.
1153 B., Alin, S., Aragão, L. E. O. C., Arneth, A., Arora, V., Bates, N. R., Becker, M., Benoit-
1154 Cattin, A., Bittig, H. C., Bopp, L., Bultan, S., Chandra, N., Chevallier, F., Chini, L. P., Evans,
1155 W., Florentie, L., Forster, P. M., Gasser, T., Gehlen, M., Gilfillan, D., Gkritzalis, T., Gregor,
1156 L., Gruber, N., Harris, I., Hartung, K., Haverd, V., Houghton, R. A., Ilyina, T., Jain, A. K.,
1157 Joetzjer, E., Kadono, K., Kato, E., Kitidis, V., Korsbakken, J. I., Landschützer, P., Lefèvre,
1158 N., Lenton, A., Lienert, S., Liu, Z., Lombardozzi, D., Marland, G., Metzl, N., Munro, D. R.,
1159 Nabel, J. E. M. S., Nakaoka, S.-I., Niwa, Y., O'Brien, K., Ono, T., Palmer, P. I., Pierrot, D.,
1160 Poulter, B., Resplandy, L., Robertson, E., Rödenbeck, C., Schwinger, J., Séférian, R.,
1161 Skjelvan, I., Smith, A. J. P., Sutton, A. J., Tanhua, T., Tans, P. P., Tian, H., Tilbrook, B., van
1162 der Werf, G., Vuichard, N., Walker, A. P., Wanninkhof, R., Watson, A. J., Willis, D.,
1163 Wiltshire, A. J., Yuan, W., Yue, X., and Zaehle, S.: Global Carbon Budget, *Earth System
Science Data* 12, 3269–3340. Friedlingstein, P., Prentice, I., 2010. Carbon-climate feedbacks:
1164 A review of model and observation based estimates. *Current Opinion in Environmental
Sustainability* 2, 251–257. <https://doi.org/10.5194/essd-12-3269-2020>, 2020.

1165
1166
1167
1168
1169 Gabrielle, B., Roche, R., Angas, P., Cantero-Martinez, C., Cosentino, L., Mantineo, M.,
1170 Langensiepen M., Hanault, C., Laville, P., Nicoulaud B., Gosse, G.: A priori
1171 parameterisation of the CERES soil-crop models and tests against several European data sets,
1172 *Agronomie* 22 (2), 119–132, <https://doi:10.1051/agro:2002003>, 2002.

1173
1174
1175 Heinen, M.: 2006. Simplified denitrification models: Overview and properties. *Geoderma*
1176 133, 444–463, <https://doi:10.1016/j.geoderma.2005.06.010>, 2006.
1177 doi:10.1016/j.geoderma.2005.06.010

1178
1179 Hidy, D., Barcza, Z., Haszpra, L., Churkina, G., Pintér, K., Nagy, Z.: 2012. Development of
1180 the Biome-BGC model for simulation of managed herbaceous ecosystems. *Ecological
Modelling* 226, 99–119, <https://doi.org/10.1016/j.ecolmodel.2011.11.008>, 2012.
1181 <https://doi.org/10.1016/j.ecolmodel.2011.11.008>

1182
1183 Hidy, D., Barcza, Z., Marjanović, H., Ostrogović Sever, M.Z., Dobor, L., Gelybó, G., Fodor,
1184 N., Pintér, K., Churkina, G., Running, S., Thornton, P., Bellocchi, G., Haszpra, L., Horváth,
1185 F., Suyker, A., Nagy, Z.: 2016. Terrestrial ecosystem process model Biome-BGCMuSo v4.0:
1186 summary of improvements and new modeling possibilities. *Geoscientific Model
Development* 9, 4405–4437, <https://doi.org/10.5194/gmd-9-4405-2016>, 2016.
1187 <https://doi.org/10.5194/gmd-9-4405-2016>

1188
1189 Hidy, D., Barcza, Z., Hollós, R., Thornton, P. and Running, S. W., Fodor, N.: User's Guide
1190 for Biome-BGC MuSo 6.2, [Available online:
1191 \[http://nimbus.elte.hu/bbgc/files/Manual_BBGC_MuSo_v6.2.pdf\]\(http://nimbus.elte.hu/bbgc/files/Manual_BBGC_MuSo_v6.2.pdf\)](http://nimbus.elte.hu/bbgc/files/Manual_BBGC_MuSo_v6.2.pdf). Available online:
1192 http://nimbus.elte.hu/bbgc/files/Manual_BBGC_MuSo_v6.2.pdf

1193
1194

1195
1196 Hufkens, K., Basler, D., Milliman, T., Melaas, E.K., Richardson, A.D.., 2018. An integrated
1197 phenology modelling framework in r. Methods in Ecology and Evolution 9, 1276–1285,
1198 <https://doi.org/10.1111/2041-210X.12970>
1199

1200 Huntzinger, D.N., Schwalm, C., Michalak, A.M., Schaefer, K., King, A.W., Wei, Y.,
1201 Jacobson, A., Liu, S., Cook, R.B., Post, W.M., Berthier, G., Hayes, D., Huang, M., Ito, A.,
1202 Lei, H., Lu, C., Mao, J., Peng, C.H., Peng, S., Poulter, B., Ricciuto, D., Shi, X., Tian, H.,
1203 Wang, W., Zeng, N., Zhao, F., Zhu, Q.., 2013. The North American Carbon Program Multi-
1204 Scale Synthesis and Terrestrial Model Intercomparison Project – Part 1: Overview and
1205 experimental design. Geoscientific Model Development 6, 2121–2133.
1206 <https://doi.org/10.5194/gmd-6-2121-2013>
1207

1208 IUSS Working Group, World Reference Base (WRB) for Soil Resources. International soil
1209 classification system for naming soils and creating legends for soil maps, World Soil
1210 Resources Reports 106, FAO, Rome, 2015.

1211
1212 Jarvis, N.J.: A simple empirical model of root water uptake, Journal of Hydrology 107, 57–
1213 72, [https://doi:10.1016/0022-1694\(89\)90050-4](https://doi:10.1016/0022-1694(89)90050-4), 1989.

1214
1215 Jones, J.W., Antle, J.M., Basso, B., Boote, K.J., Conant, R.T., Foster, I., Godfray, H.C.J.,
1216 Herrero, M., Howitt, R.E., Janssen, S., Keating, B.A., Munoz-Carpena, R., Porter, C.H.,
1217 Rosenzweig, C., Wheeler, T.R.., 2017. Brief history of agricultural systems modeling. Agricultural
1218 Systems 155, 240–254, <https://doi.org/10.1016/j.agrosy.2016.05.014>, 2017.
1219 <https://doi.org/10.1016/j.agrosy.2016.05.014>
1220

1221 Keenan, T.F., Carbone, M.S., Reichstein, M., Richardson, A.D.., 2011. The model–data
1222 fusion pitfall: assuming certainty in an uncertain world. Oecologia 167, 587–597.
1223 <https://doi.org/10.1007/s00442-011-2106-x>
1224 *

1225
1226 Kern, A., H.–Marjanović, H.–and Z.– Barcza, Z.., 2016. Evaluation of the quality of NDVI3g
1227 dataset against Collection 6 MODIS NDVI in Central-Europe between 2000 and 2013. Remote
1228 Sensing 8 (11), 955, <https://doi.org/10.3390/rs8110955>, 2016.
1229 doi:10.3390/rs8110955
1230

1231 Koven, C.D., Riley, W.J., Subin, Z.M., Tang, J.Y., Torn, M.S., Collins, W.D., Bonan, G.B.,
1232 Lawrence, D.M., Swenson, S.C.., 2013. The effect of vertically resolved soil
1233 biogeochemistry and alternate soil C and N models on C dynamics of CLM4. Biogeosciences
1234 10, 7109–7131, <https://doi.org/10.5194/bg-10-7109-2013>, 2013.<https://doi.org/10.5194/bg-10-7109-2013>
1235

1236
1237 Kuzyakov, Y.., 2011. How to link soil C pools with CO₂ fluxes? Biogeosciences 8, 1523–
1238 1537, <https://doi.org/10.5194/bg-8-1523-2011>, 2011.<https://doi.org/10.5194/bg-8-1523-2011>
1239

1240 Levis, S.., 2010. Modeling vegetation and land use in models of the Earth System. WIREs
1241 Climate Change 1, 840–856. <https://doi.org/10.1002/wcc.83>,
1242 <https://doi.org/10.1002/wcc.83>
1243

1244 Marek, G. W., Evett, S. R., Gowda, P. H., Howell, T. A., Copeland, K. S., Baumhardt, R. L..,

1245 , 2014. Post-processing techniques for reducing errors in weighing lysimeter
1246 evapotranspiration (ET) datasets. American Society of Agricultural and Biological Engineers
1247 57, 499–515. <https://doi.org/10.13031/trans.57.10433>,
1248 [2014https://doi.org/10.13031/trans.57.10433](https://doi.org/10.13031/trans.57.10433).
1249

1250 Martínez-Vilalta, J., Sala, A., Asensio, D., Galiano, L., Hoch, G., Palacio, S., Piper, F.I.,
1251 Lloret, F., 2016. Dynamics of non-structural carbohydrates in terrestrial plants: a global
1252 synthesis. Ecological Monographs 86, 495–516, <https://doi.org/10.1002/ecm.1231>, 2016.
1253 <https://doi.org/10.1002/eem.1231>
1254

1255 Martre, P., Wallach, D., Asseng, S., Ewert, F., Jones, J.W., Rötter, R.P., Boote, K.J., Ruane,
1256 A.C., Thorburn, P.J., Cammarano, D., Hatfield, J.L., Rosenzweig, C., Aggarwal, P.K.,
1257 Angulo, C., Basso, B., Bertuzzi, P., Biernath, C., Brisson, N., Challinor, A.J., Doltra, J.,
1258 Gayler, S., Goldberg, R., Grant, R.F., Heng, L., Hooker, J., Hunt, L.A., Ingwersen, J.,
1259 Izaurralde, R.C., Kersebaum, K.C., Müller, C., Kumar, S.N., Nendel, C., O’leary, G., Olesen,
1260 J.E., Osborne, T.M., Palosuo, T., Priesack, E., Ripoche, D., Semenov, M.A., Shcherbak, I.,
1261 Steduto, P., Stöckle, C.O., Stratonovitch, P., Streck, T., Supit, I., Tao, F., Travasso, M., Waha,
1262 K., White, J.W., Wolf, J., 2015. Multimodel ensembles of wheat growth: many models are
1263 better than one. Global Change Biology 21, 911–925. <https://doi.org/10.1111/gcb.12768>,
1264 [2015.https://doi.org/10.1111/geb.12768](https://doi.org/10.1111/geb.12768)
1265

1266 McMahon, T.A., Peel, M.C., Lowe, L., Srikanthan, R., McVicar, T.R., 2013. Estimating
1267 actual, potential, reference crop and pan evaporation using standard meteorological data: a
1268 pragmatic synthesis. Hydrology and Earth System Sciences 17, 1331–1363.
1269 <https://doi.org/10.5194/hess-17-1331-2013>.
1270

1271 Medlyn, B.E., Dreyer, E., Ellsworth, D., Forstreuter, M., Harley, P.C., Kirschbaum, M.U.F.,
1272 Le Roux, X., Montpied, P., Strassemeyer, J., Walcroft, A., Wang, K., Loustau, D., 2002.
1273 Temperature response of parameters of a biochemically based model of photosynthesis. II. A
1274 review of experimental data. Plant, Cell & Environment 25, 1167–1179.
1275 <https://doi.org/10.1046/j.1365-3040.2002.00891.x>, 2002.
1276 <https://doi.org/10.1046/j.1365-3040.2002.00891.x>
1277

1278 Merganičová, K., Merganič, J., Lehtonen, A., Vacchiano, G., Sever, M.Z.O., Augustynczik,
1279 A.L.D., Grote, R., Kyselová, I., Mäkelä, A., Yousefpour, R., Krejza, J., Collalti, A., Reyer,
1280 C.P.O., 2019. Forest carbon allocation modelling under climate change. Tree Physiology
1281 39, 1937–1960. <https://doi.org/10.1093/treephys/tpz105>, 2019.
1282 <https://doi.org/10.1093/treephys/tpz105>
1283

1284 Olin, S., Schurgers, G., Lindeskog, M., Wårlind, D., Smith, B., Bodin, P., Holmér, J., Arneth,
1285 A., 2015. Modelling the response of yields and tissue C:N to changes in atmospheric CO₂
1286 and N management in the main wheat regions of western Europe. Biogeosciences 12, 2489–
1287 2515, <https://doi.org/10.5194/bg-12-2489-2015>, 2015. <https://doi.org/10.5194/bg-12-2489-2015>
1288

1289 Parton, W.J., Holland, E., Del Grosso, S., Hartman, M., Martin, R., Mosier, A.R., Ojima, D.,
1290 Schimel, D., 2001. Generalized model for NO_x and N₂O emissions from soils. Journal of
1291 Geophysical Research: Atmospheres, 106, 17403–17419, [2001](https://doi.org/10.1029/2000JD20001).
1292

1293 Pásztor, L., Laborczi, A., Takács, K., Illés, G., Szabó, J., and Szatmár, G.,
1294

1295 Szatmári, 2020. Progress in the elaboration of GSM conform DSM products and their
1296 functional utilization in Hungary. *Geoderma Regional* 21,
1297 <https://doi.org/10.1016/j.geodrs.2020.e00269>, ISSN 2352-0094,
1298 <https://doi.org/10.1016/j.geodrs.2020.e00269>

1299

1300 Pavelka, M., Acosta, M., Kiese, R., Altimir, N., Brümmer, C., Crill, P., Darenova, E., Fuß, R.,
1301 Gielen, B., Graf, A., Klemedtsson, L., Lohila, A., Longdoz, B., Lindroth, A., Nilsson, M.,
1302 Marañon-Jimenez, S., Merbold, L., Montagnani, L., Peichl, M., Pihlatie, M., Pumpanen, J.,
1303 Serrano Ortiz, P., Silvennoinen, H., Skiba, U., Vestin, P., Weslien, P., Janouš, D., and Kutsch, W.: Standardisation of chamber technique for CO₂, N₂O and CH₄ fluxes measurements from
1304 terrestrial ecosystems. *International Agrophysics*, 32(4), 569-587
1305 <https://doi.org/10.1515/intag-2017-0045>, 2018.

1306

1307

1308 Peaucelle, M., Janssens, I., Stocker, B., Ferrando, A., Fu, Y., Molowny-Horas, R., Ciais, P.,
1309 Penuelas, J., 2019. Spatial variance of spring phenology in temperate deciduous forests is
1310 constrained by background climatic conditions. *Nature Communications* 10, 5388,
1311 <https://doi.org/10.1038/s41467-019-13365-1>, 2019. <https://doi.org/10.1038/s41467-019-13365-1>

1312

1313

1314 Rawls, J., Onstad, W., A. Richardson, H., 1980. Residue and Tillage Effects on SCS Runoff
1315 Curve Numbers. *Transactions of the ASAE* 23, 357-0361,
1316 <https://doi.org/10.13031/2013.34585>. <https://doi.org/10.13031/2013.34585>

1317

1318 Richardson, A.D., Keenan, T.F., Migliavacca, M., Ryu, Y., Sonnentag, O., Toomey, M., 2013. Climate change, phenology, and phenological control of vegetation feedbacks to the
1319 climate system. *Agricultural and Forest Meteorology* 169, 156-173,
1320 <https://doi.org/10.1016/j.agrformet.2012.09.012>, 2013.
1321 <https://doi.org/10.1016/j.agrformet.2012.09.012>

1322

1323

1324 Ritchie, J.T., 1998. Soil water balance and plant water stress. in: Tsuji, G.Y., Hoogenboom,
1325 G., Thornton, P.K. (Eds.): *Understanding Options for Agricultural Production*, Springer
1326 Netherlands, Dordrecht, pp. 41-54, https://doi.org/10.1007/978-94-017-3624-4_3, 1998.
1327 https://doi.org/10.1007/978-94-017-3624-4_3

1328

1329 Ritchie, J.T., 1981. Water dynamics in the soil-plant-atmosphere system. *Plant and Soil*, 58,
1330 81-96, <https://doi.org/10.1007/BF02180050>, 1981. <https://doi.org/10.1007/BF02180050>

1331

1332 Running, S., Hunt, E.R., 1993. Generalization of a forest ecosystem process modelForest
1333 Ecosystem Process Model for other biomesOther Biomes, BIOME-BGC, and an
1334 applicationApplication for global-scale models. In: Scaling Physiological Processes:
1335 Leaf to Globe, edited by J. R. Ehleringer and C. Field, pp. 141-158, Academic Press,
1336 San DiegoRunning Global Scale Models.

1337 Running, S.W., Gower, S.T., 1991. FOREST-BGC, A general model of forest ecosystem
1338 processes for regional applications. II. Dynamic carbon allocation and nitrogen
1339 budgets. <https://doi.org/10.1093/treephys/9.1-2.147>,
1340 1993. <https://doi.org/10.1093/treephys/9.1-2.147>

1341

1342 Sándor, R., Barcza, Z., Acutis, M., Doro, L., Hidy, D., Köchy, M., Minet, J., Lellei-Kovács,
1343 E., Ma, S., Perego, A., Rolinski, S., Ruget, F., Sanna, M., Seddaiu, G., Wu, L., Bellocchi, G.,
1344 2017. Multi-model simulation of soil temperature, soil water content and biomass in Euro-

1345 Mediterranean grasslands: Uncertainties and ensemble performance. *European Journal of*
1346 *Agronomy* 88, 22–40, <https://doi.org/10.1016/j.eja.2016.06.006>, 2017.
1347 <https://doi.org/10.1016/j.eja.2016.06.006>

1348

1349 Schwalm, C., Schaefer, K., Fisher, J., Huntzinger, D., Elshorbany, Y., Fang, Y., Hayes, D.,
1350 Jafarov, E., Michalak, A., Piper, M., Stofferahn, E., Wang, K., Wei, Y., 2019. Divergence in
1351 land surface modeling: Linking spread to structure. *Environmental Research*
1352 *Communications* 1, 111004, <https://doi.org/10.1088/2515-7620/ab4a8a>, 2019.
1353 <https://doi.org/10.1088/2515-7620/ab4a8a>

1354

1355 Smith, N.G., Dukes, J.S., 2013. Plant respiration and photosynthesis in global-scale models:
1356 incorporating acclimation to temperature and CO₂. *Global Change Biology* 19, 45–63.
1357 <https://doi.org/10.1111/j.1365-2486.2012.02797.x>, 2013. <https://doi.org/10.1111/j.1365-2486.2012.02797.x>

1356

1357 Thomas, Q., Bonan, G., Goodale, C., 2013. Insights into mechanisms governing forest
1358 carbon response to nitrogen deposition: A model–data comparison using observed responses
1359 to nitrogen addition. *Biogeosciences* 10, 3869–3887, <https://doi.org/10.5194/bg-10-3869-2013>.
1360 <https://doi.org/10.5194/bg-10-3869-2013>

1361

1362

1363

1364 Thornton, P.E., Rosenbloom, N.A., 2005. Ecosystem model spin-up: Estimating steady state
1365 conditions in a coupled terrestrial carbon and nitrogen cycle model. *Ecological Modelling*
1366 189, 25–48. <https://doi.org/10.1016/j.ecolmodel.2005.04.008>,
1367 <https://doi.org/10.1016/j.ecolmodel.2005.04.008>

1368

1369

1370 Tillman, F.D., Weaver, J.W., 2006. Uncertainty from synergistic effects of multiple
1371 parameters in the Johnson and Ettinger (1991) vapor intrusion model. *Atmospheric*
1372 *Environment* 40, 4098–4112, <https://doi.org/10.1016/j.atmosenv.2006.03.011>, 2006.
1373 <https://doi.org/10.1016/j.atmosenv.2006.03.011>

1374

1375 USDA, https://www.nrcs.usda.gov/Internet/FSE_DOCUMENTS/stelprdb1044818.pdf, 1987.

1376

1377 USDA, 1987. https://www.nrcs.usda.gov/Internet/FSE_DOCUMENTS/stelprdb1044818.pdf

1378 Verbeeck, H., Samson, R., Verdonck, F. and Lemeur, R., 2006. Parameter sensitivity and
1379 uncertainty of the forest carbon flux model FORUG: a Monte Carlo analysis. *Tree*
1380 *Physiology* 26, 807–817, 2006.

1381

1382 Vetter, M., Churkina, G., Jung, M., Reichstein, M., Zaehle, S., Bondeau, A., Chen, Y., Ciais, P.,
1383 Feser, F., Geyer, R., Jones, C., Papale, D., Tenhunen, J., Tomelleri, E., Trusilova, K.,
1384 Viovy, N., Heimann, M., 2008. Analyzing the causes and spatial pattern of the European
1385 2003 carbon flux anomaly in Europe using seven models. *Biogeosciences Discussions*, v.4,
1386 1201–1240 (2007) 5, <https://doi.org/10.5194/bg-5-561-583>. <https://doi.org/10.5194/bg-5-561-2008>, 2008.

1387

1388

1389 Wallace, J.S., Holwill, C.J., 1997. Soil evaporation from tiger-bush in south-west Niger. *Journal of Hydrology* 188–189, 426–442. [https://doi.org/10.1016/S0022-1694\(96\)03185-X](https://doi.org/10.1016/S0022-1694(96)03185-X),
1390 [https://doi.org/10.1016/S0022-1694\(96\)03185-X](https://doi.org/10.1016/S0022-1694(96)03185-X)

1391

1392

1393 White, M., Thornton, P., Running, S., Nemani, R., 2000. Parameterization and sensitivity
1394 analysisSensitivity Analysis of the Biome-BIOME-BGC terrestrial ecosystem model: net

1395 [primary production controls, Terrestrial Ecosystem Model: Net Primary Production Controls.](https://doi.org/10.1175/1087-3562(2000)004<0003:PASAOT>2.0.CO;2)
1396 Earth [Interact. Interactions—EARTH INTERACT 4, 1-85, https://doi.org/10.1175/1087-3562\(2000\)004<0003:PASAOT>2.0.CO;2](https://doi.org/10.1175/1087-3562(2000)004<0003:PASAOT>2.0.CO;2), 2000.. [https://doi.org/10.1175/1087-3562\(2000\)004<0003:PASAOT>2.0.CO;2](https://doi.org/10.1175/1087-3562(2000)004<0003:PASAOT>2.0.CO;2)

1397
1398
1399
1400
1401
1402
1403
1404
1405
1406
1407
1408
1409
1410
1411
1412
1413
1414
1415
1416
1417
1418

Widen, B., Lindroth, A.: A Calibration System for Soil Carbon Dioxide – Efflux Measurement Chambers: Description and Application. *Soil Science Society of America Journal*. 67, 327-334., <https://doi.org/10.2136/sssaj2003.0327>, 2003.

Woodrow, I., Berry, J. [2003.](https://doi.org/10.1146/annurev.pp.39.060188.002533) Enzymatic Regulation of Photosynthetic CO₂, Fixation in C3 Plants. *Annual Review of Plant Physiology and Plant Molecular Biology* 39, 533–594.
<https://doi.org/10.1146/annurev.pp.39.060188.002533>

Zimmermann, M., Leifeld, J., Schmidt, M.W.I., Smith, P., Fuhrer, J. [2007.](https://doi.org/10.1111/j.1365-2389.2006.00855.x) Measured soil organic matter fractions can be related to pools in the RothC model. *European Journal of Soil Science* 58, 658–667. <https://doi.org/10.1111/j.1365-2389.2006.00855.x>

Zhen, M., Tang, J., Li, C., Sun. H.: [Rhamnolipid-modified biochar-enhanced bioremediation of crude oil-contaminated soil and mediated regulation of greenhouse gas emission in soil.](https://doi:10.1007/s11368-020-02746-5) *Journal Soils Sediments* 21, 123–133. <https://doi:10.1007/s11368-020-02746-5>, 2021.